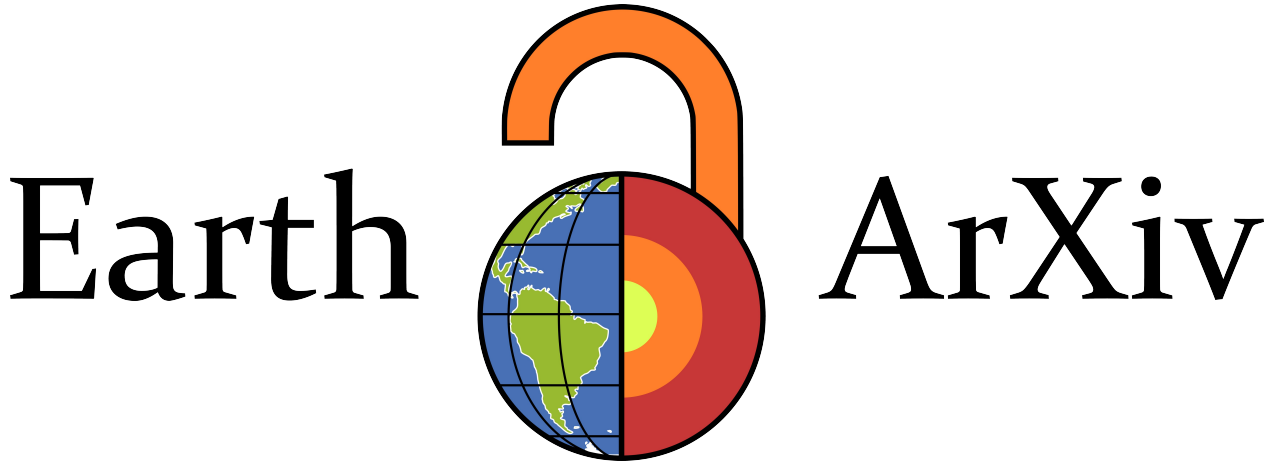

Thermo-Hydraulic Optimization of Deep Geothermal Systems: Computational Methods and Classification

Ulrich Steindl [*] *Thomas Hamacher* [†] *Smajil Halilovic* [‡]

Chair of Renewable and Sustainable Energy Systems,
Technical University of Munich, Germany

Abstract

Deep geothermal energy forms an important part of a sustainable energy portfolio, providing baseload power and heat. A significant global expansion of deep geothermal systems (DGSs) is projected for the coming decades, thereby increasing use of local geothermal resources. This, together with a competitive energy market, creates an incentive to optimize DGSs with respect to large-scale design and operational control variables. In particular, simulation-based optimization can enhance both the sustainability and economic viability of geothermal projects. Key decisions include well placement, well spacing, flow rates, and reinjection temperatures, all of which interact through the coupled thermo-hydraulic behavior of the reservoir. This review provides an overview of thermo-hydraulic optimization methods for DGSs, with a focus on computational simulation-optimization pipelines. The reviewed literature is organized according to a newly proposed classification scheme; for each study, the underlying model, optimization methodology, and objective functions are reported. Finally, open challenges and research directions in the field are identified.

Keywords: deep geothermal systems, thermo-hydraulic modeling, simulation-based optimization, well placement, surrogate models, porous media flow

1 Introduction

The global production of geothermal energy is steadily increasing–both for electricity generation and direct use. According to Lund et al. [1], the installed thermal capacity of the various applications amounted to 107.7 GW by 2020, comprising energy generation from deep and shallow geothermal systems. While heat pumps account for 71.6% of the

[*]ORCID: 0009-0003-9501-5984, Corresponding author. E-mail address ulrich.steindl@tum.de (U. Steindl)
[†]ORCID: 0000-0002-0387-8199
[‡]ORCID: 0000-0002-2024-8201

installed capacity, the remaining 28.4% are mostly DGSs [1]. Due to their higher production temperature, DGSs play an increasingly important role in global efforts to achieve a sustainable and carbon-neutral district heating supply. Accordingly, the installed capacity for space heating increased by more than 50% between 2015 and 2020 [1].

The construction of DGSs within the vicinity of urban areas with high population density and advantageous geological features is particularly promising. This is due to the critical number of potential customers that promote the economically viable construction of a local heating network [2]. In addition, at present, the transportation of hot water and steam over long distances is not feasible [3, 4]. This further limits the available geothermal resources to those located in close proximity to consumers.

As a result, deep geothermal energy systems are expected to draw increasingly on aquifers near urban areas. Examples already include the Dogger aquifer around Paris [5], the Molasse basin around Munich [6], and the Xianxian geothermal field [7].

The intensive use of geothermal resources comes with risks regarding their sustainable management. In the early history of the deep geothermal energy exploitation, the produced water was not reinjected into the reservoir. To this day in thermal water production for balneology, reinjection is not always obligatory [8]. This practice frequently results in overexploitation due to the emerging pressure losses [9]. Furthermore, the disposal of substantial volumes of brine in lakes and rivers leads to environmental damages [10–12]. Reinjecting the heat-depleted water back into the aquifer stabilizes the pressure field and is therefore the industry-wide standard [13, 14].

Cold fluid reinjection into the reservoir produces cold-water plumes migrating towards the production well [15]. Therefore, a potential issue is the occurrence of *thermal breakthroughs*, meaning that cold water is cycled between injection and production well. Positioning injection and production wells close to each other increases the risks of an early thermal breakthrough [16, 17]. Opposed to this, large well distances may prevent temperature declines at production wells, but can lead to the aforementioned pressure losses [18]. As a result of improper well spacing, economic performance is diminished, since the cost of provided heat rises with lower temperatures and higher pumping rates (cf. Section 4.3).

Given the aforementioned issues, a strong case exists for properly planning, i.e., optimizing new DGSs regarding crucial design and operation specifications. Besides well spacing, the economic and technical performance of a geothermal system is influenced by several factors, including extraction and injection temperature, well depths, and pumping pressure [15, 19]. Geothermal energy is often –especially in the context of space heating– exploited by doublet systems [20]. Even the design and operation optimization of a doublet system is a non-trivial task [9]. Multi-well systems and multi-doublet systems are also studied [21–23] and realized [24]. Compared to doublets, the complexity of such systems is further pronounced by the increased number of design variables, which adds to the optimization challenge.

Although there is a well-established practice of simulating reservoirs [25–27], and geothermal plants [28] through thermo-hydraulic (TH) models in great detail, mathematical optimization for DGSs is less studied. Mathematical design and operation optimization uses systematic methods to maximize or minimize specific performance indicators.

This process is crucial in many scenarios, such as:

1. The design optimization of a new geothermal system in an aquifer where other systems are already operational in order to maximize the total power output of all systems.
2. Design and operation optimization for a multi-well DGS project to extract the maximum heat energy from an aquifer.
3. Two-level optimization of several deep geothermal systems together with a district heating network.

The DGS optimization literature contains prior studies addressing similar scenarios [3, 22, 29, 30]. However, a substantial number of contributions merely compare disparate, predefined scenarios of design and operation conditions.

Regarding subject-related overview articles, a perspective paper by Rajabi et al. [31] identifies an incentive for utilizing machine learning (ML) methods for DGS design optimization. Pandey et al. [26] provide a comprehensive overview of geothermal reservoir modeling; however, they do not address the topic of optimization. Özkaraca [32] reviews optimization methods for geothermal power generation, but focuses on the optimization of the thermodynamic cycle and usage of surface equipment, whereas our study focuses on the subsurface design. Halilovic et al. [33] categorize different optimization approaches for the design of open-loop shallow geothermal systems. To the best of our knowledge, this is the first ever study to systematically review the topic of thermo-hydraulic design and operation optimization for conventional DGSs.

This paper provides a comprehensive overview of the relevant literature on the design optimization of DGSs. Accordingly, it evaluates extant approaches to DGS optimization, with an emphasis on the strengths and limitations of these methods. In addition, a novel classification system is proposed for the integrated simulation-optimization approaches in DGS engineering. Finally, we explore potential research directions culminating in a state-of-the-art overview on the subject.

The paper is structured as follows: Section 2 begins with a review of terminology about conventional DGS. Section 3 presents the TH models underpinning geothermal system optimization. This is followed by a review of the components of an optimization problem, with examples from DGS optimization in Section 4. The main section of the document comprises a comprehensive review and classification of available literature concerning the optimization of geothermal system designs (cf. Section 5). Additionally, we provide a preliminary localization of methods regarding their computational cost and discuss the advantages and limitations of the considered optimization studies. The paper concludes

by examining the limitations of the extant literature and exploring the potential research directions that emerge from it in Sections 6–7.

2 Conventional Deep Geothermal Systems

The categorization of geothermal systems has been attempted based on various criteria such as temperature ranges [34], permeabilities and geological play types [35], and methods of energy extraction [36]. The sources underlying economically viable subsurface heat reservoirs range from the regular geothermal gradient to shallow magma. Together with the present geological facies, they govern the formation of geothermal reservoirs and, in turn, the applicable energy extraction methods [36]. As a result, a rich but often inconsistent terminology has developed in scientific and technical discourse.

This paper uses terminology developed in a paper by Khodayar and Björnson [36], which divides geothermal systems into *conventional* and *unconventional*. As such, the term DGS refers to conventional geothermal systems hereafter. Such systems are characterized by favorable geological subsurface conditions, featuring viable heat sources, fluid, and high rock permeabilities at depths within drilling range. The physical criteria for conventional reservoirs are temperatures up to 374 °C, pressures below 221 bar and a maximum drilling depth of 3.5 km [36]. Under these conditions, hot fluid can be exploited solely through conventional well drilling and pumping. Reservoirs exceeding conventional temperatures and pressures are classified as unconventional because under these conditions water acts as a corrosive fluid, complicating the energy extraction.

This paper is concerned with optimization methods for the main subsurface features of (conventional) DGSs, excluding the optimization of surface equipment and thermodynamic cycles. Therefore, our definition of a DGS includes the combination of subsurface technical installations such as wells and pumps and the geological formations hosting the hot fluid. This definition of conventional DGS aligns well with the scope of the present literature review on geothermal system design optimization based on TH models.

Our working definition therefore explicitly excludes unconventional geothermal systems, such as engineered or enhanced geothermal systems (EGSs), and ultra-deep applications. The optimization of EGSs requires a different modeling approach, where rock-mechanical processes and artificial fracture creation are of primary importance in the design process [37, 38].

The most basic exploitation setup involves a *doublet scheme*–i.e., one production well and one reinjection well (cf. Figure 1)–drilled into the target formation. The hot fluid is extracted from the aquifer at the production well and transferred through a heat exchanger or a generator. After heat extraction, the cooled water is reinjected into the aquifer via the injection well. Depending on the formation pressure and the fluid temperature, appropriately dimensioned pumps may be required to maintain flow in the production and reinjection wells [36].

The cost structure of a DGS project can be roughly divided into *capital expenditure*

C^{CAPEX} and *operational expenditure* C^{OPEX}. The central portion of C^{CAPEX} comes from well drilling [39] and the installation of pumps and surface equipment [3, 40]. The C^{OPEX} is primarily determined by electricity costs during the operation and the maintenance costs of the pumps. Therefore, the flow rate of the plant at a given pumping pressure is a critical factor determining the economic viability of a DGS project [41]. Low flow rates—encountered during reservoir exploration or after system commissioning—are therefore one of the main investment risks. Some studies provide minimal permeability or transmissivity thresholds for economically viable operation. For example, Bauer et al. [8] claim that a minimum transmissivity of 0.0002 m^2/s is required for a 700 kW pumping system to achieve economically viable flow rates in a carbonate reservoir, while Khodayar and Björnson [36] provide a permeability range of $0.1 - -250$ mD for a magmatic-source DGS to be economically viable.

On the revenue side, income from a DGS project is determined by the thermal energy output and the market price of heat or electricity. Medium- and high-temperature systems (100–374 °C [36]) allow for higher-value applications, such as power generation or supplying industrial process heat. Depending on the reservoir temperature, different heat extraction methods are used to produce steam or hot water [36, 42]. For power generation, flash plants are commonly used, where steam is separated from thermal water and fed into a turbine [36]. In heating applications, hot water is sent through a heat exchanger, from which the energy is distributed [43]. Low-temperature systems (< 100 °C) are typically used for district heating or heat pump projects [36], which often have lower profit margins [44].

A temperature decline during operation that drops below acceptable levels may require supplemental heat sources or, in the worst case, render the plant economically unviable [13]. Thus, low fluid temperature due to reservoir heat depletion is another principal investment risk for conventional geothermal projects [45].

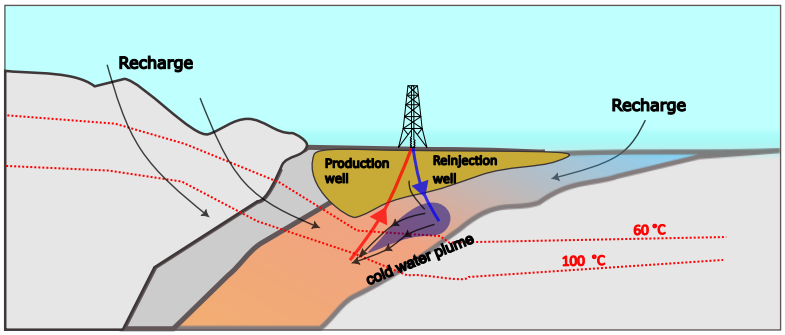

Fig. 1: **Schematic of a DGS with a production and an injection well.** Simplified and compiled from [35, 36].

Exploiting geothermal energy is a complex task that requires a detailed understanding of the underlying physical processes and geological risks. Modeling the installation

beforehand—regarding expected productivity and temperature—is critical to assess the economic viability. Additionally, optimal system design becomes crucial as geothermal projects often operate on low profit margins compared to fossil fuel projects [46]. To this end, accurate geothermal reservoir models are essential for evaluating how the well pattern design and plant operation influence both productivity and temperature of the extracted fluid.

3 Underlying Thermo-Hydraulic Models

The application of mathematical optimization to the problem of geothermal energy extraction relies on the prior development of a robust mathematical model $\mathcal{M}$. Classically, the modeling of geothermal reservoirs is founded on the hypothesis that they are primarily porous media, as described by the continuum approach. In this description, the microscopic features of the medium, such as the precise pore structure, are substituted by a representative elementary volume (REV) [47].

The REV is the smallest volume above which a measurement of macroscopic continuum mechanical material properties is independent of the size of the volume. As a result, mechanical and thermal material bulk properties serve as an approximation of the material's exact structure (cf. Table 2) [47–49]. As such, material properties of the porous medium κ form an essential part of the model parameters θ of the mathematical model $\mathcal{M}$.

Implementing a mathematical model depends on establishing a conceptual model of the aquifer. A comprehensive conceptual model is a descriptive model that includes the geometry of the study area, the geological facies, and their corresponding physical properties together with knowledge about the relevant physical processes [47, 50]. In a more refined stage, a conceptual model can be represented as a three- or two-dimensional raster grid, to which the material properties are assigned. Many simulation software solutions offer utilities for creating conceptual models from geological data, often in combination with maps of the study area [51, 52]. Especially in case studies for geothermal system planning, highly resolved conceptual models are employed to maximize the precision [7, 28, 53]. Nevertheless, methodological studies grounded in rudimentary, homogeneous aquifer models prove pertinent in understanding the principles underlying the optimization of geothermal system design [18, 22, 54].

The continuum theoretical abstraction of the conceptual model is a domain $\Omega \subseteq \mathbb{R}^{2,3}$ in three or two dimensions, where the state variables $\mathbf{s}(\mathbf{x}, t)$ of the porous medium are defined as mathematical functions over space $\mathbf{x} \in \Omega$ and time $t \in (0, \infty)$. In the domain of geothermal engineering, particularly within the framework of DGS optimization, the primary objective is to compute the spatio-temporal evolution of pressure $p(\mathbf{x}, t)$, Darcy velocity $\mathbf{q}(\mathbf{x}, t)$, and temperature field $T(\mathbf{x}, t)$ in Ω, that is $\mathbf{s} = (T, p, \mathbf{q})$. Since the state variables describe subsurface conditions, they cannot be measured directly.

Therefore, developing a proper mathematical model is necessary to explain and predict

reservoir behavior. Such a model takes in the model parameters (MPs) θ, and outputs the state variables $\mathcal{M}(\theta) = \mathbf{s}$ by solving a set of governing equations. At this stage, the general porous media theory uses partial differential equations (PDEs) that govern processes in the aquifer Ω [47].

The solutions to these equations form the foundation for the optimization of DGSs, since the predicted temperature and hydraulics in the aquifer can be used to extract data for the key technical and economic performance metrics of the system. As such, the accuracy of the employed TH model naturally limits the accuracy of the optimization. The precision of TH models depends on a multitude of factors including –but not limited to– the considered physical processes, quality of the input data, and, for numerical solutions, on the discretization. Several studies have delineated the difficulties of geothermal reservoir modeling [25, 26]. The following sections present the governing equations and the most prominent approximation methods for solutions of DGS.

3.1 Governing Equations

The most general mathematical description of a geological subsurface system considers the principal macroscopic physical and chemical processes. These are thermal (T), hydraulic (H), mechanical (M), and chemical (C) processes, each of which is governed by different PDEs. Furthermore, these processes are coupled; for example, the temperature field influences the pressure field through the fluid density and viscosity [55]. However, in TH processes, which are normally considered for DGSs optimization, one neglects the mechanical and chemical processes (cf. Figure 2).

A TH model $\mathcal{M}$ of an aquifer with a geothermal plant is a set of governing equations that describe the temporal and spatial evolution of $\mathbf{s} = (T, p, \mathbf{q})$. These equations are subject to the aquifer's initial and boundary conditions β (cf. Section 3.1.1) and material properties κ. To maintain simplicity in the analysis, deep aquifers are often assumed to be confined and fully saturated with a single fluid, such as water [48].

The pressure can be computed by solving the mass and momentum conservation equation, which in the *Boussinesq approximation* reads,

$$S\frac{\partial p}{\partial t} + \nabla\cdot\frac{\mathbf{K}}{\mu}\Big(-\nabla p + \rho^f \mathbf{g}\Big) = Q^f. \tag{1}$$

Here, S is the storativity coefficient, $\mathbf{K}$ the permeability tensor of the aquifer, μ the dynamic viscosity of the fluid, ρ^f the density of the fluid and $\mathbf{g}$ the vector of gravitational force [48, 56]. Additionally, Q^f are the sources and sinks of mass, including the processes of production and reinjection.

The *Darcy velocity* $\mathbf{q}$ is the vector field corresponding to the pressure gradient and represents the velocity field of fluid particles moving through the aquifer [47, 48]. Thus, the *Darcy equation* reads

$$\mathbf{q} = \frac{\mathbf{K}}{\mu}(-\nabla p + \rho^f \mathbf{g}). \tag{2}$$

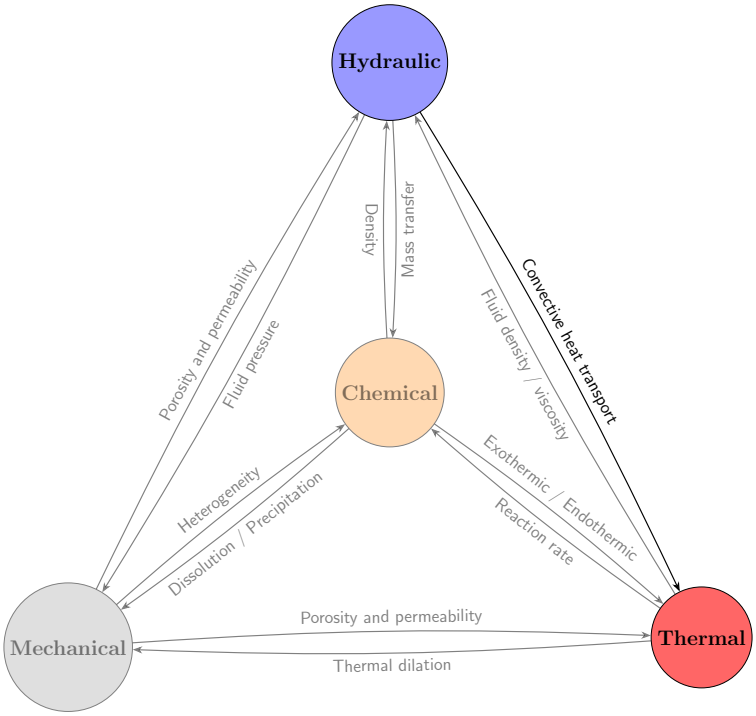

Fig. 2: **Coupling between chemical and physical processes in a geothermal reservoir.** Greyed-out processes are generally not considered in the context of DGS optimization. Reproduced from Tao et al. [55]

The heat transport in the reservoir is governed by a sum of diffusion and advection mechanisms, resulting in the *advection-diffusion equation* [47, 48], which reads

$$\rho C \frac{\partial T}{\partial t} + \rho^f c^f \mathbf{q} \cdot \nabla T - \nabla \cdot (\mathbf{\Lambda} \nabla T) = Q^t. \tag{3}$$

Here, ρC is the combined volumetric heat capacity of the solid and liquid phase, namely (cf. Table 2)

$$\rho C = \epsilon \rho^f c^f + (1 - \epsilon) \rho^s c^s. \tag{4}$$

Furthermore, Q^t represents sources and sinks of thermal energy, usually geothermal reinjection wells or naturally present subsurface heat sources. In addition, $\mathbf{\Lambda}$ denotes the weighted thermodispersion tensor of the combined materials [48], that is

$$\mathbf{\Lambda} = \left(\epsilon \lambda^f + (1 - \epsilon) \lambda^s\right) \mathbb{I} + \epsilon \rho^f c^f \mathbf{D}_{\text{mech}}.$$

Expanding the mechanical dispersion tensor gives

$$\mathbf{D}_{\text{mech}} = \eta_T \|\mathbf{q}\| \mathbb{I} + (\eta_L - \eta_T) \frac{\mathbf{q} \otimes \mathbf{q}}{\|\mathbf{q}\|}$$

with η_L being the longitudinal and η_T the transversal thermodispersion [48]. The remaining parameters may be found in Table 2.

The PDEs (1)–(3) above are the core equations in TH modeling. It should be noted that besides the material properties κ, additional input parameters are necessary for a realistic and solvable model. Firstly, the efficient mathematical description of the source terms, the wellbores, is essential. Secondly, it is imperative to specify the initial state of the problem to ensure its well-posedness. Lastly, in the case of non-homogeneous or anisotropic aquifer models, the distribution of material parameters matching borehole observations is crucial. These modeling aspects are discussed in detail in the following subsections.

3.1.1 Boundary Conditions

To ensure the existence and uniqueness of solutions, it is necessary to supply values for the state variables arising in Equations (1) and (3) on the boundary of the modeling domain, denoted by $\partial\Omega$. Furthermore, in the case of time-dependent problems, it is necessary to assign initial values to state variables at the initial time, $t = 0$. In the mathematical literature, these problems are formally classified as *boundary value* (BVP) or *initial value problems* (IVP) for time-dependent problems. The corresponding solutions, in turn, can be approximated through analytical or numerical methods.

For example, to solve Equation (1), one has to prescribe the pressure solution p at the boundary of the aquifer as a *Dirichlet boundary condition* $\bar{p}$ or the Darcy velocity $\mathbf{q}$ of the fluid at the boundary as a *Neumann boundary condition* $\bar{\mathbf{q}}$.

$$\begin{aligned} \text{Dirichlet BC:} \quad & \forall \mathbf{x} \in \partial\Omega,\, t \in [t_0, t_1] \quad p(\mathbf{x}, t) = \bar{p}(\mathbf{x}, t) \\ \text{Neumann BC:} \quad & \forall \mathbf{x} \in \partial\Omega,\, t \in [t_0, t_1] \quad \mathbf{q}(\mathbf{x}, t) = \bar{\mathbf{q}}(\mathbf{x}, t) \end{aligned}$$

In the context of the advection-diffusion equation, the prescribed temperature or heat flux at the boundary is designated as either Dirichlet or Neumann boundary conditions, respectively.

Furthermore, a critical component of geothermal engineering is modeling the mass and heat sources, Q^f and Q^t, respectively. These quantities describe the thermal and hydraulic influence of production and injection wells. Since wellbores are several orders of magnitude smaller than the aquifer scale, a numerical resolution (cf. Section 3.2.1) is not computationally feasible for large-scale reservoir models. Thus, the wellbore is modeled as either a line source or as a point source coinciding with the edges or vertices of the mesh, respectively. As such, wells can be incorporated into the model as singular well-type boundary conditions [48]. Although such assumptions constitute a simplification, the loss in accuracy can be mitigated by modeling heat loss in the wellbore separately [57].

Alternative approaches to modeling source terms — specifically mollified Dirac delta functions — have been proposed to enhance flexibility in optimization. This method, used by Blank et al. [22], decouples the source location from mesh nodes, making it suitable for optimization workflows. The derivation of physically consistent boundary and initial conditions from field data is discussed in the following subsection on inverse modeling.

3.1.2 Inverse Modeling

A central challenge in applying the governing equations to real-world geothermal systems is ensuring that the model accurately reflects field conditions. Accordingly, a *calibrated model* $\mathcal{M}(\theta)$ should reproduce measurements of the state variables $\mathbf{s}(\mathbf{x}_1, t_1), \ldots, \mathbf{s}(\mathbf{x}_n, t_n)$. The model calibration is connected to the following two questions:

1. How to identify appropriate boundary conditions?
2. How should spatially distributed parameters—such as permeability, porosity, and thermal conductivity—be estimated?

A common calibrating process answers these questions by adjusting the estimated material parameters κ and boundary conditions β to align model output with borehole measurements [58]. Addressing this issue is challenging in TH modeling and forms a part of the *inverse modeling* process. Calibration techniques are widely used in the literature, particularly for case studies involving prediction of real-world aquifers [7, 53].

Mathematically, inverse modeling can be formulated as an optimization problem minimizing the discrepancy between simulated and observed data. Given that measurements up to a certain degree can be explained by both the MPs and the boundary conditions, the inverse model problem is usually ill-posed [59]. In addition, a considerable computational cost is associated with the inverse modeling process, which arises from the optimization of MPs [60].

3.2 Approximating Solutions of the Governing Equations

The solutions to the governing equations can be approximated using various methods, which will be reviewed in the following subsections. First, a discretization can be introduced, and the equations can be solved numerically. Second, the PDEs may be simplified and solved analytically by introducing various assumptions. A third approach involves surrogate models, which are black-box models trained on the output of a numerical model.

Because BVPs can only be solved analytically in very special cases, numerical and surrogate methods are the main methods in the simulation of complex DGSs. The computational expense of these methods varies, and is qualitatively ranked in Figure 3, indicating that the lowest costs are caused by analytical models, followed by surrogate models, and the highest computational cost is due to numerical models.

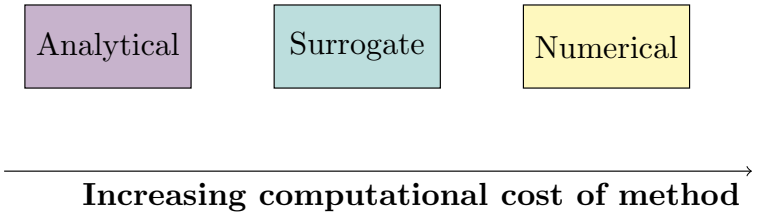

Fig. 3: **Comparison of computational costs by underlying modeling method.**

3.2.1 Numerical Models

In the case of numerical methods, the governing equations are discretized into a finite number of spatial elements and time steps to achieve a numerical solution. In this process, the PDEs are converted into a system of matrix equations that can be solved by a computer.

Numerous software packages are available for the numerical simulation of all aspects of the THMC processes in geothermal systems. Bundschuh and Suárez [47] provide a comprehensive overview of software solutions and their particular capabilities. The most common spatial discretization schemes (Figure 4) in numerical treatment of PDE include the finite difference method (FDM), finite volume method (FVM), and finite element method (FEM) [61].

The **finite difference method (FDM)** is conceptually the most straightforward approach. It relies on Taylor series expansions to approximate derivatives over a regular grid, typically composed of quadratic cells. Multiple applications supporting geothermal modeling, such as the reservoir simulator ECLIPSE [62] utilize computation kernels based on FDM. While FDM is computationally efficient and relatively straightforward to implement, it is limited in geometric flexibility. Complex geological features, such

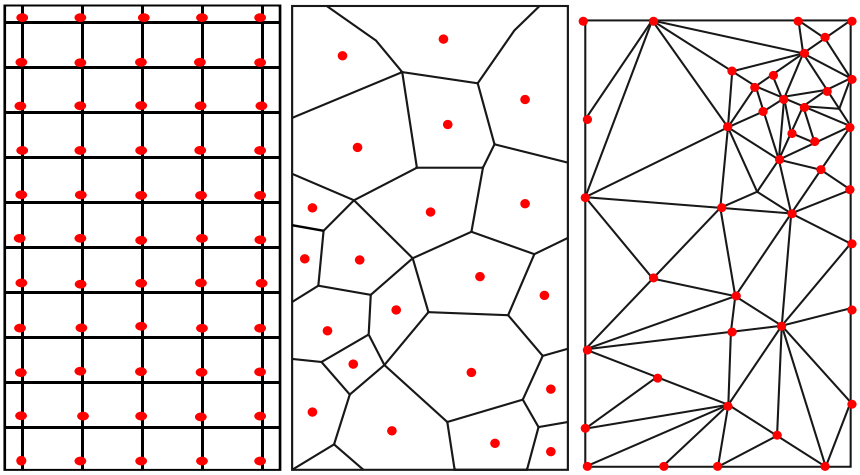

Fig. 4: **Schematic of the three most common discretization schemes in geothermal modeling.** From left to right: FDM, FVM, FEM; Red dots indicate the location where the functions are evaluated. The polygons delimit the approximating cells for the corresponding methods.

as faults or inclined wellbores, are challenging to represent. Moreover, FDM does not inherently conserve physical quantities such as mass and energy [61].

The **finite volume method (FVM)** improves on these limitations by discretizing the governing equations over control volumes rather than points. Fluxes are computed at the faces of each volume, enabling exact conservation of mass and energy within each cell. FVM supports unstructured meshes, providing greater geometric flexibility than FDM, although it is still somewhat constrained in the case of highly complex domains. Its computational cost generally falls between that of FDM and FEM. An example of FVM-based software is TOUGH2, a numerical simulator for non-isothermal multiphase flow in porous and fractured media [63, 64].

The **finite element method (FEM)** is the most flexible and computationally intensive of the three schemes. FEM relies on a weak formulation of the PDEs, expressing the solution in terms of basis functions over elements. This approach supports highly irregular meshes and variable resolution, making it well-suited for modeling complex subsurface geometries. When adequately formulated, FEM maintains conservation properties and often exhibits higher-order convergence than FDM or FVM [61]. It is widely used in applications where local refinement and accurate boundary representation are critical. There are several numerical simulators dedicated to THMC modeling based on FEM, such as FEFLOW [48], the MOOSE/GOLEM framework [65], and OpenGeoSys [52].

3.2.2 Analytical Models

Prior to the advent of computer-aided numerical models, analytical expressions describing the evolution of the states $\mathbf{s} = (T, p, \mathbf{q})$ were employed to estimate the behavior of

underground fluids. As PDE (1) and (3) are well-known from other engineering disciplines, analytical solutions from fields such as material sciences are available [49, 66].

The seminal contribution in hydrology due to Theis [67] is an analytical formula for the *hydraulic head* near a continuously pumping well with flow rate Q^f. The hydraulic head, denoted by h, is defined as the height of a water column that would exert a hydrostatic pressure equal to the pressure in the aquifer at the bottom of the well. It is related to the pressure p by the equation

$$p = \rho^f g(h - z), \tag{5}$$

where z is the elevation above the reference level and g is the gravitational acceleration. Theis' approach is founded on the premise of a homogeneous, confined, isotropic, infinitely large aquifer, with the well operating at a constant flow rate. In the most elementary approximation, the analytical solution for the hydraulic head drawdown Δh at a radius r and time t reads

$$\Delta h(r,t) = \frac{Q^f}{4\pi\tau}\Big(- \gamma - \ln\Big(\frac{r^2 S}{4\tau t}\Big)\Big) \tag{6}$$

where γ is the Euler-Mascheroni constant and τ the transmissivity (cf. Table 2) [47, 49]. A variant of the Theis solution is also employed for aquifers with distinct hydraulic conductivities in an optimization study by Tselepidou [68].

The solution proposed by Theis is a variation of the infinite line source solution. Complementarily, the finite line source solution is a concept of particular relevance. This solution is a reliable method for describing the hydraulic head drawdown of a well that does not fully penetrate the aquifer. The stationary hydraulic head drawdown in with respect to the flowrate $Q^f$is thus expressed as follows:

$$\Delta h(r,z) = \int_\Gamma \frac{Q^f}{4\pi\tau\big((z-\zeta)^2 + r^2\big)^{1/2}} d\zeta, \tag{7}$$

where z is the vertical coordinate, Γ the well, and ζ the depth of the well [49, 69].

Equally, heat transport in porous media was studied through analytical methods as early as the 1950s. An early example is a paper by Lauwerier [70] within the context of crude oil reservoirs. In addition, the analytical description of the cold water plume, generated by a reinjection well, has received considerable attention [29, 71–74].

A widely cited contribution due to Bodvarsson [71] describes the thermal influence of wells injecting cold water into a fracture. In the proposed model, the cold water plume within the fracture is advected by a homogeneous flow field, neglecting conduction. Thermal conduction describes the temperature distribution in the adjacent rock matrix. This model is especially suitable for high-permeability reservoirs located above volcanic heat sources. The solution for the temperature at a distance r from the reinjection well is given by

$$T(r,t) = T^0 \cdot \operatorname{erf}\big(\frac{\pi b r^2 + y}{2\sqrt{at}}\big). \tag{8}$$

In this equation, a is the thermal diffusion coefficient of the rock, erf is the error function, and b is a factor containing the flow rate to permeability ratio. Moreover, T^0 is the initial temperature and y is the vertical distance from the fracture [71].

Analytical models have been also used in optimization studies, such as the seminal work by Gringarten and Sauty [29]. A two-dimensional aquifer vertical model is employed with a series of simplifying assumptions. The researchers propose an analytical expression for the minimal injection-production well spacing at which no thermal interference occurs during an operational time, denoted by Δt. The formula, given by the positive solution of

$$D^2 = 2Q^f \Delta t \cdot \left(\beta h + \left(\beta^2 h^2 + \alpha \Delta t\right)^{\frac{1}{2}}\right)^{-1} \tag{9}$$

supports the intuition that the well spacing D should be increased with the flow rate Q^f and the operational time Δt. The parameters α and β depend on porosity and heat capacity.

Birdsell et al. [75] use analytical solutions for the heat equation in combination with the 1-dimensional Darcy equation to evaluate reservoir impedance and production temperature for different well layouts. In addition, they develop a model for the approximate evaluation of reservoir pressure resulting from reinjection.

Despite their reduced generalizability and precision compared to numerical models, analytical models possess several advantages. These models are characterized by their ease of implementation and interpretation, with minimal computational requirements. Furthermore, the coupling of analytical models with gradient-based optimization methods is straightforward, enabling computationally efficient optimization schemes. However, although analytical solutions offer valuable insights and computational efficiency, their applicability is often limited to simplified scenarios. They can serve as benchmarks or initializations for more comprehensive numerical or surrogate-based optimization frameworks (cf. Section 4).

3.2.3 Surrogate Models

A *surrogate model* is a mathematical model that serves as a secondary model or partial black-box model of a complex system [76]. These models are designed to be computationally efficient compared to—in our case—numerical simulations of an aquifer, while still reproducing the principal outcomes of the complex model.

In the context of simulating TH effects, a surrogate model aims to approximate the mapping from initial conditions and material parameters to the space of state variables defined by the governing equations (1)–(3). If $\mathcal{M}(\theta) = (T, p, \mathbf{q})$ is a solution of the governing equations obtained, for example, through a numerical method depending on a parameter set θ, then a surrogate model $\tilde{\mathcal{M}}$ approximates the mapping

$$\theta \mapsto (T, p, \mathbf{q}).$$

The key difference from numerical methods is that, depending on the approximation strategy, only parts of the physical theory are used. In this sense, surrogate models can be classified into three major categories according to Asher et al. [77].

The first category consists of **data-driven surrogates**. Typically, a data-driven model is a function of the MPs θ, and a set of *weights* ϕ that are adjusted during a training process [77]. Data-driven models are trained on high-fidelity numerical simulations or field measurements and log data. A trained model can then be used to predict the state variables for another interpolated parameter set θ', i.e.,

$$\tilde{\mathcal{M}}(\phi)(\theta') \approx (T, p, \mathbf{q})(\theta'). \tag{10}$$

These data-driven models do not use information about the mathematical structure of the underlying equations. Such an approximation is normally only valid if θ' lies within the interpolation range of the training data.

The surrogate type dictates the functional form and parametrization of $\tilde{\mathcal{M}}$ and the number of model weights ϕ. Data-driven surrogates span a spectrum from simple parametric models such as low-order polynomials, including response surface models (RSMs), to non-parametric models such as Gaussian processes regression (GPR), regression trees, or artificial neural networks (ANNs) [77, 78]. Especially RSMs are fundamental tools in design and operational optimization of DGSs [44, 79]. Basic feed-forward neural network (FFNN) architectures have been applied in DGS modeling and optimization but were limited in generalization capabilities and accuracy [80]. Typical challenges of data-driven TH surrogates include the significant computational expense associated with training data generation and, regarding the model capacity, overfitting or too few parameters.

Recent advances in artificial intelligence, especially in deep learning, have contributed to addressing several of these challenges. Particularly, neural networks that incorporate parts of the physical theory –known as physics-informed neural networks (PINNs)– have gained significant attention in modeling porous media [81]. They represent a promising approach toward overcoming limitations of pure data-driven methods [82], with the additional advantage of producing physically meaningful solutions [82]. Moreover, PINNs have recently found application in geothermal system optimization, as shown in a publication by Yan et al. [54]. Another prominent neural network architecture is Long-Short-Term Memory (LSTM) networks, which are particularly suited for time-dependent modeling tasks [83].

Beyond purely data-driven approaches, **physics-based reduction techniques** constitute another primary class of surrogates. Therefore, the second surrogate model category identified by Asher et al. comprises **projection-based** (POD) and **reduced-basis methods** (RB). In these approaches, the governing equations are projected onto a low-dimensional subspace represented by an orthonormal basis of solutions. These bases are generated from single simulations (snapshots) of high-resolution numerical models. This technique is widely used in the geoscientific community and is applied for reservoir-scale

simulations and data inversion techniques, such as magnetotelluric data. A comprehensive overview of available work on POD and RB methods is given by Degen et al. [84].

The third and final surrogate model type described by Asher et al. [77] is **multi-fidelity simulation**. In addition to the fine discretization, two coarser grids are employed to efficiently compute, for example, pressure on the fine grid. To the authors' knowledge, RB/POD methods and multi-fidelity simulations have not yet been applied to geothermal system optimization. However, there are many other engineering applications where design optimization is combined with lower-resolution simulations, for example, optimal airfoil design [85].

In summary, geoscientific and particularly geothermal reservoir simulations revolve around the fundamental trade-off between the accuracy of mathematical models and their computational and structural complexity. This trade-off is particularly relevant for deep geothermal system optimization, where repeated forward simulations are often required in the context of design exploration and uncertainty quantification. Given the computational demand of simulating geothermal reservoirs, surrogate models can replace these forward simulations. As such, surrogate models can serve as key tools for enabling efficient design and optimization workflows. In the following sections, we will explore how the simulation models serve as a basis for relevant design and operational optimization in deep geothermal system engineering.

4 Optimization Approaches

A common engineering problem is finding the *optimal* parameters of a process, subject to certain constraints. Such tasks generally can be reformulated as extreme value problems of mathematical functions representing a performance metric of the process. An optimization is the automated mathematical procedure of finding the solution of such an extreme value problem.

Two major categories of optimization problems are optimal design problems (ODPs) and optimal control problems (OCPs). In ODPs, the *design variables* are time-independent, whereas OCPs additionally involve time-dependent *control variables*. Both are special cases of general optimization problems (OPs), which may combine stationary and time-dependent variables. Examples for ODPs are aerodynamic design optimization in aviation [86, 87] or, more specifically, wind turbine blade shape optimization [88]. Examples for OCPs are found in model-predictive control problems [89], such as in chemical process control [90] and optimal dispatch of power units [91–93].

Historically, heuristics have proven adequate for the design and control of DGSs. However, with the increasing deployment density of new DGSs (cf. Section 1), the placement and operation of new geothermal wells are important thermo-hydraulic ODPs and OCPs, respectively. The goal of such an optimization is the improvement of technical or economic metrics without compromising the feasibility of the design.

To this end, we study the mathematical setup of a generic OP. An OP consists of a set of

possibly constrained *control* or *design variables* $\mathbf{d} = (d_1, \ldots, d_n) \in \mathbb{R}^n$ and an *objective function* $\mathcal{F}(\mathbf{d})$. In general, an optimization problem can be expressed mathematically as

$$\begin{aligned} \text{minimize} \quad & \mathcal{F}(\mathbf{d}) && (11)\\ \text{subject to} \quad & \mathbf{f}(\mathbf{d}) \leq 0 && (12)\\ & \mathbf{g}(\mathbf{d}) = 0 && (13) \end{aligned}$$

where the Equations 12–13 are the *inequality* ($\mathbf{f}$) and *equality constraints* ($\mathbf{g}$), respectively [94, 95]. In engineering applications, the computation of the objective $\mathcal{F}$ often requires evaluating a simulation model. The model $\mathcal{M}$ depends on MPs θ, such as porous media properties and the optimization variables (OVs) $\mathbf{d}$. Such a model-based approach is called the *simulation-optimization approach* [96] or *simulation-based optimization* [97].

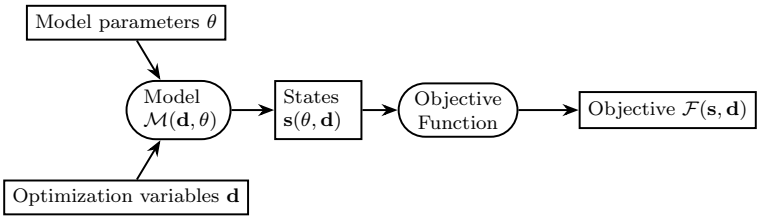

Fig. 5: **Basic computation steps for the simulation-optimization approach for DGSs.** The model $\mathcal{M}$ is evaluated for a given optimization variable $\mathbf{d}$ and model parameters θ to compute the state variables $T, p, \mathbf{q}$. The objective function $\mathcal{F}$ is then computed based on the state and optimization variables.

For DGSs, one optimization step requires the evaluation of one of the aforementioned thermo-hydraulic models (Section 3). The basic computational pipeline is depicted in Figure 5. It starts with two data sources for the underlying model of a geothermal installation and the geothermal reservoir. One data source are the MPs, which remain fixed during optimization of a conventional DGS design. Another data source are the OVs, which are explained in Section 4.1. The initial values of the optimization variables must be supplied manually and are updated as the optimization progresses.

This input is fed into the TH model to compute the relevant state variables. Subsequently, these state variables are used to extract information about the quality of the design, that is, the value of the objective function. The typical objectives occurring in optimizing geothermal systems are explained in Section 4.3. The state variables and optimization variables are restricted by the *constraints* (Section 4.2) bounding the set of feasible designs. Finally, the *optimization algorithm* (cf. Section 4.4) automatically updates the optimization variables. To simplify the following discussion, we exclusively consider the case of a minimization problem and note that a maximization problem can be transformed into a minimization problem by negating the objective function.

4.1 Optimization Variables

The optimization variables $\mathbf{d} \in D$ are the mathematical parameters incrementally adjusted during the optimization. A globally optimal design or control $\mathbf{d}^\star$ is a choice of optimization variables $\mathbf{d}$ that solves the optimization problem. Particularly, for a minimization problem, we have

$$\forall \mathbf{d} \in D \quad \mathcal{F}(\mathbf{d}^\star) \leq \mathcal{F}(\mathbf{d})$$

where D is the set of all feasible designs (Section 4.2).

As such, a choice of values for $\mathbf{d} = (d_0, \ldots, d_n)$ uniquely corresponds to a real-world design. The number of optimization variables n represents the dimensionality of the problem. In effect, every design variable adds degrees of freedom (DoFs) and increases the computational cost and the complexity of the numerical optimization.

The choice of proper variables is indispensable for a well-posed optimization scenario: The OVs must not be determined by the evaluation of the objective function; that is, they have to remain fixed during the evaluation of the forward problem [95]. Furthermore, a choice of OVs has to point uniquely to a corresponding realization of a design. The functional form of the problem sometimes depends on the coordinate system in which the OVs are represented. As such, an appropriate choice of OV representation can resolve computational difficulties by exploiting symmetries to reduce dimensions or resolve nonlinearity. Finally, the objective function must be sensitive to the OVs, i.e., changes in design variables should produce measurable changes in the objective [95].

In practice, DGS design is bounded by two conditions: the available geothermal resource (aquifer depth, thermal gradient, permeability) and the projected heat demand. Optimization then seeks the best configuration of design and operational variables to bridge supply and demand efficiently. Depending on the value range, these OVs can be classified into *discrete* and *continuous*. At the level of the governing equations, this translates to finding the optimal placement and time-varying strengths of source terms in the mass conservation law, Equation (1), and the advection-diffusion equation, Equation (3).

Design variables in DGS optimization

- number of production and reinjection wells n_{pr}, n_{in} (discrete)
- positions $\mathbf{x}_1^{in}, \ldots \mathbf{x}_{n_{in}}^{in}, \mathbf{x}_1^{pr}, \ldots, \mathbf{x}_{n_{pr}}^{pr} \in \Omega$ inside the aquifer (continuous)
- depth of the wells $z_1^{in}, \ldots, z_{n_{in}}^{in}, z_1^{pr}, \ldots, z_{n_{pr}}^{pr}$ (continuous)

Complementarily, the control variables determine the strength of the source terms in the governing equations.

Control variables in DGS optimization

- flow rates of the wells $q_1, \ldots, q_{n_{in}+n_{pr}}$ (continuous)
- pumping pressure of the wells $p_1, \ldots, p_{n_{in}+n_{pr}}$ (continuous)

- injection temperature of the cooled water $T_1^{in}, \ldots, T_{n_{in}}^{in}$ (continuous)

With a sufficiently accurate model, these OVs can be used to evaluate the fundamental performance parameters of different designs.

In addition to the previous design variables, one can define derived design variables. For example, the well spacing $d(\mathbf{x}_i^{in}, \mathbf{x}_j^{pr})$ [18], which is the distance between the injection well $\mathbf{x}_i^{in}$ and the production well $\mathbf{x}_j^{pr}$. Also investigated are multi-well configurations, based on grid and polygon arrangements Γ [22, 53]. For such configurations, the sizing and the orientation angle ϕ of the basic polygon and grid shapes are the respective design variables.

By introducing derived design variables, the number of OVs can be reduced and, thus, computational efficiency enhanced. Constraining equations can be introduced to further restrict the search space, which will be discussed in the next section.

4.2 Optimization Constraints

There are two main categories of constraints, *hard* and *soft constraints*. Hard constraints, on the one hand, arise as model equations (e.g., Darcy's equation governing reservoir pressure). Furthermore, design limitations such as the upper limit of technically feasible drilling ranges constitute a hard constraint. Collectively, the constraints $\mathbf{f}, \mathbf{g}$ (cf. Equation (12)–(13)) directly or implicitly restrict the design space to a *feasible region* D, defined as the subset of designs $\mathbf{d}$ that satisfy all hard constraints.

Soft constraints, on the other hand, impose a penalty on the objective function. For example, the temperature drop along the model boundary of a DGS model is a soft constraint for operational controls. Likewise, maximum drilling costs (or drilling range) are soft constraints for a design, penalizing it if they exceed a certain value. Soft constraints are introduced into the optimization by adding a weighted penalty term for the constraint violation to the objective.

The key implication of this distinction is admissibility: hard constraints define the boundary of the feasible region D and must never be violated, while soft constraints trade violation against objective performance via a penalty weight. This allows constrained problems to be solved with unconstrained methods, at the cost of tuning the penalty.

4.3 Objective Functions

The optimization objective is the functional $\mathcal{F}$, which corresponds to the target quantity of the optimization problem. Depending on the optimization scenario, $\mathcal{F}$ is minimized (or maximized) by the optimization algorithm. The evaluation cost $\mathcal{F}(\mathbf{d})$ fundamentally determines the computational complexity of the optimization problem. In the optimization of DGSs, the computational demand is primarily determined by the coupled simulation model [95].

A crucial property is the objective function's *regularity*, defined by the number of continuous derivatives. Higher regularity enables the application of efficient gradient-based algorithms to the optimization problem. If $\mathcal{F}$ is not differentiable, gradient-free algorithms may be the only option, increasing the computational cost of the optimization (cf. Section 4.4).

The *modality* of the objective function — the number of optimal points — is another crucial factor (cf. Figure 6). The optimization problem may have a global optimum, multiple global optima, or only local optima, where global optima $\mathbf{d}^\star$ satisfy

$$\mathcal{F}(\mathbf{d}^\star) = \min_{\mathbf{d} \in D} \mathcal{F}(\mathbf{d}).$$

Objectives with more than one optimum are *multimodal*, whereas objectives with only one are *unimodal*. If the optimization goal is to find a global optimum, multimodal problems are more complicated to solve than unimodal problems. The reason is that optimization algorithms can get stuck in a local extremum, requiring additional strategies to avoid such issues [95]. A special case of unimodal problems are *convex* OPs, where the objective function is convex. This class is well-studied, and efficient algorithms exist to solve such optimization tasks [94]. A further important aspect is multi-objective opti-

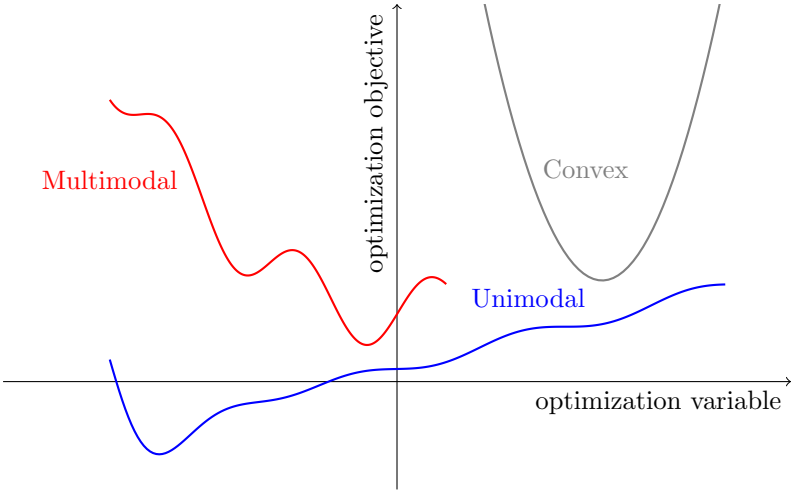

Fig. 6: **Illustration of the modality of an objective function.** The objective function is unimodal if it has only one extremum, and multimodal otherwise. Reproduced from Martins et al. [95].

mization (MOO), where multiple objectives are optimized simultaneously. In this case, the objective function is vector-valued $\mathcal{F}(\mathbf{d}) = (f_1(\mathbf{d}), \ldots, f_m(\mathbf{d}))$. *Pareto optimality* is a key concept in MOO: a solution $\mathbf{d}$ is *Pareto optimal* if there is no other solution $\mathbf{d}'$ such that $f_i(\mathbf{d}') \leq f_i(\mathbf{d})$ for all i and $f_j(\mathbf{d}') < f_j(\mathbf{d})$ for at least one j. This is particularly relevant when there is a trade-off between different objective functionals [95].

In the following, we present a selection of objectives from the DGS optimization literature, beginning with technical performance metrics.

4.3.1 Technical performance objectives

A fundamental task of DGS engineering is achieving optimal energy extraction with the available resources. Several technical performance metrics quantify the thermal energy output of the DGS. The most direct objective is maximizing the bottom-hole temperature of production wells $T^{bh} = T(\mathbf{x}^{pr})$. Closely related is the *well head temperature* T^{wh} of the production wells, which is derived from the bottom-hole temperature by considering the heat loss along the wellbore [57]. Many publications on DGS optimization analyze the effect of the OVs on T^{wh} or T^{bh} [7, 80, 98].

The well-head temperature T^{wh} is directly related to the thermal energy that can be extracted from the system. The instantaneous produced thermal power is described by the expression $W^{th}(t) = C_v \cdot q_k(t) \cdot (T^{wh}(t) - T^{in}(t))$ where T^{in} is the injection temperature [79]. For an array of n production and injection wells, the cumulative thermal energy output is given by

$$E^{th} = \sum_{k=1}^{n} \int_{t_0}^{t_l} q_k \cdot C_v \cdot \eta_t \cdot (T_k^{wh}(t) - T_k^{in}(t))dt \tag{14}$$

where q_k is the flow rate of the k-th production well and η_t is the efficiency of the heat exchange. For power generation, the power output can be estimated by the thermal energy output multiplied by the conversion efficiency of the power plant η_e. As such, the thermal energy output is a common objective function in DGS optimization [44, 54].

Deep geothermal systems often require a minimal production temperature. If a thermal breakthrough occurs, i.e., T^{wh} drops below this threshold temperature, the system may become unprofitable or even infeasible. Temperature dependence is especially critical for power generation, since the related energy conversion processes are temperature dependent [99]. Therefore, a common optimization objective in the literature is maximizing the time t^b before the thermal breakthrough occurs [30, 100].

The second major class of technical objectives concerns efficient fluid extraction from the DGS. The hydraulic head $h(\mathbf{x}_{pr})$ near a production well is the key determinant of well productivity. Sustainable production requires the hydraulic head drawdown $\Delta h = h(\mathbf{x}^{pr}, t_0) - h(\mathbf{x}^{pr}, t_1)$ during the operation time interval (t_0, t_1) to be minimal. Excessive drawdown reduces well productivity — since flow rate is proportional to the hydraulic head gradient by Darcy's law — and increases pump energy demand. In multi-well systems, large drawdowns can also cause interference between neighbouring wells or contribute to aquifer over-depletion. Optimal well placement has been studied by multiple authors to minimize the hydraulic head drawdown [101–103].

Another fundamental quantity is the bottom-hole pressure difference of a production-injection well pair, given by $\Delta p = p(\mathbf{x}^{pr}) - p(\mathbf{x}^{in})$ [44]. Various derived performance

indicators are based on Δp. The key indicator is the pump power required to drive the system at a given flow rate. One possibility to quantify this dependency is the *reservoir impedance* $\mathcal{I}$ that results from the pressure difference Δp of a production-injection well pair [75].

$$\mathcal{I} = \frac{\Delta p}{q} \tag{15}$$

Here q is the volumetric or mass flow rate of the system. The inverse $\mathcal{I}^{-1}$ is the *productivity index* and is also considered in the literature [28].

Low reservoir impedances reduce the pump energy required to achieve a given flow rate q, making fluid extraction more efficient. However, excessively low reservoir impedance can lead to a hydraulic breakthrough, such that reinjected cold water is directly advected to the production well.

Complementary to the energy output, the power consumption of the pumps can be estimated from the pressure difference and flow rate. The instantaneous power consumption of the pumps can be approximated by the formula

$$W^{pump} = \frac{\Delta p \cdot q}{\eta_p}. \tag{16}$$

where η_p is the efficiency of the pump system [19]. Additionally, the total electricity E^{pump} consumed by the DGS is given by time integration of the above equation. The net energy generated by the system is then given by [22, 104]

$$E^{net} = E^{th} - E^{pump}. \tag{17}$$

The ratio of harvested thermal energy to consumed electrical energy is an essential measure for the efficiency of a DGS. Therefore, another optimization objective is the *coefficient of performance*

$$CoP = \frac{E^{th}}{E^{pump}} \tag{18}$$

which quantifies the installation's efficiency in producing thermal energy [98, 104].

To assess overall resource utilization, some authors optimize the ratio of produced to theoretically available energy in the reservoir

$$R^g = \frac{E^{th}}{\int_\Omega \rho C \cdot (T^0 - T^{in}) d\Omega} \tag{19}$$

where T^0 is the unperturbed reservoir temperature and ρC is the combined heat capacity as in Equation 4 [53, 100, 104].

4.3.2 Economic performance objectives

While technical metrics quantify physical performance, economic objectives assess the financial viability of a DGS project. They are structured around the balance between project costs and revenues from energy sales. On the cost side, a distinction is made between the initial capital cost $\mathrm{C}^{\mathrm{CAPEX}}$ required to realize a design, and the recurring operational costs. The latter are dominated by pump energy consumption; together with maintenance expenses, they constitute the annual operation and maintenance costs $\mathrm{C}_{\mathrm{t}}^{\mathrm{OPEX}}$ [103]. The revenues generated by energy sales over the system's lifetime LT represent the income side. Balancing the costs and income of a DGS yields the annual *cash flow* CF_t defined as

$$\begin{aligned} \mathrm{CF}_0 &= E_0^e \cdot \mathrm{C}_0^e - \mathrm{C}^{\mathrm{CAPEX}} - \mathrm{C}_0^{\mathrm{OPEX}} \\ \mathrm{CF}_t &= E_t^e \cdot \mathrm{C}_t^e - \mathrm{C}_{\mathrm{t}}^{\mathrm{OPEX}} \quad \text{for } t = 1, \ldots, LT \end{aligned} \tag{20}$$

where E_t^e with $e = el, th$ is produced energy and C_t^e is the price of one energy unit. The *cumulated cash flow* (CCF) [105] over the lifetime of a plant has been used as optimization objective [106].

In energy system analysis, it is common to discount future cash flows to account for the time value of money [107]. To this end, capital costs $\mathrm{C}^{\mathrm{CAPEX}}$ are balanced with the discounted annual cash flows of the DGS project, yielding the fundamental investment metric, the *net present value*

$$\mathrm{NPV} = -\mathrm{C}^{\mathrm{CAPEX}} + \sum_{t=1}^{LT} \frac{\mathrm{CF}_t}{(1+i)^t} \tag{21}$$

with an interest rate i. Wees et al. [108] analyzed the NPV for deep geothermal systems; Kahrobaei et al. [109] optimized it. Chen et al. [110] recently conducted an optimization for the NPV without annuities.

From the NPV, various analyses on the system's economic viability can be derived [107]. To compute the break-even point for the profitability of the system, we set NPV to zero and assume that the energy price $C_{e,t} = C$ is constant. Solving for C yields the *Levelized Cost of Energy* (LCOE) [111], which reads

$$\mathrm{LCOE} = \frac{\mathrm{C}^{\mathrm{CAPEX}} + \sum_{t=0}^{LT} \mathrm{C}_{\mathrm{t}}^{\mathrm{OPEX}} \cdot (1+i)^{-t}}{\sum_{t=0}^{LT} E_t^e \cdot (1+i)^{-t}} \tag{22}$$

Depending on the type of energy produced, the LCOE can be interpreted as the cost per unit of heat (LCOH) or electricity. The LCOE is an important benchmark for the economic competitiveness of a DGS and has been considered by various authors [30, 53, 103].

The additional costs due to pressure loss at the production well and thermal breakthrough are also considered as optimization objectives. To capture these effects, increased power consumption and temperature decline of the extracted fluid are combined

into the cumulative additional production cost, described by

$$\mathrm{C}^{\mathrm{add}} = \sum_{t=0}^{N} E_t^{el} \cdot \mathrm{C}_t^{el} + E_t^{th} \cdot \mathrm{C}_t^{th}. \tag{23}$$

The additional electricity costs may be estimated by simulating the pressure loss at the production well. Moreover, in the original paper by Kong et al. and other literature, annuities are included [7, 18, 83] similarly to the net present value (Eq. 21).

In summary, it is important to choose an objective function aligned with the optimization goal. While engineers may be primarily interested in technical efficiency, economic viability is equally important. One scenario is optimizing the NPV to meet an investor's return expectations; another is minimizing the LCOE to be competitive on the energy market.

The next section presents the mathematical means for reaching the optimization goal. We shall review the types of algorithms for iterating over the optimization variables and their corresponding strengths and weaknesses.

4.4 Optimization algorithms

An optimization algorithm formally consists of a sequence of calculation steps updating the optimization variables until a termination criterion is met. Depending on the method, each iteration requires the evaluation of the objective function and possibly its gradients. Figure 7 shows a broad classification of optimization algorithms based on the use of derivative information, search scheme, and evaluation method.

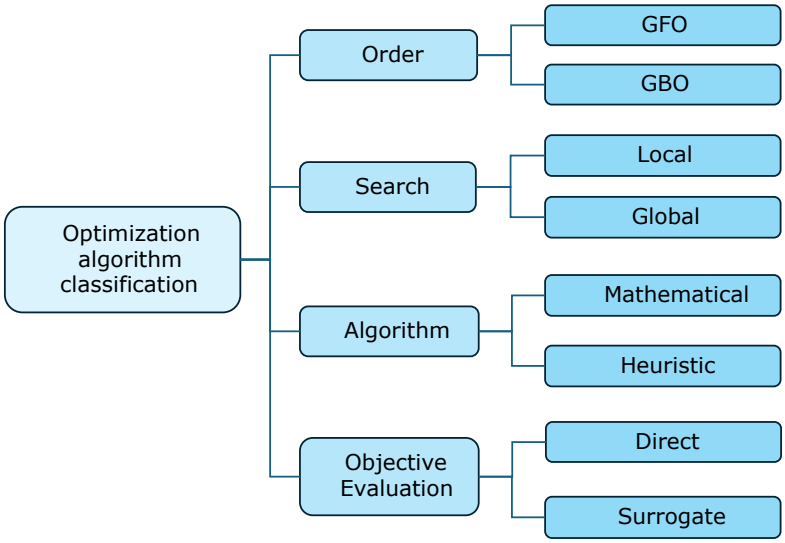

Fig. 7: **Classification of optimization algorithms.** Adapted from Martins et al. [95].

gradient-free optimizers (GFOs) are zero-order methods, meaning that they rely on objective function evaluations only. Unlike GFOs, gradient-based optimizers (GBOs) require the objective function and constraints to be differentiable. They use the gradients of the objective function $\frac{\partial \mathcal{F}}{\partial d_i}$ and constraints $\frac{\partial \mathbf{c}}{\partial d_i}$. The gradients are used to compute the *search direction* in which the optimization variables are updated, scaled by the step length. The required regularity increases with the method's order. For example, when using classical first-order methods (e.g., gradient descent), the problem is required to be once continuously differentiable [94], whereas modern algorithms are less restricted [112].

GBOs have several practical advantages over GFOs. First, the number of required function evaluations scales roughly linearly with the number of design variables for GBOs [95], while GFOs scale exponentially with the number of design variables (cf. Figure 8). For complex problems with many design variables, this means a difference of many orders of magnitude in the number of evaluations [95].

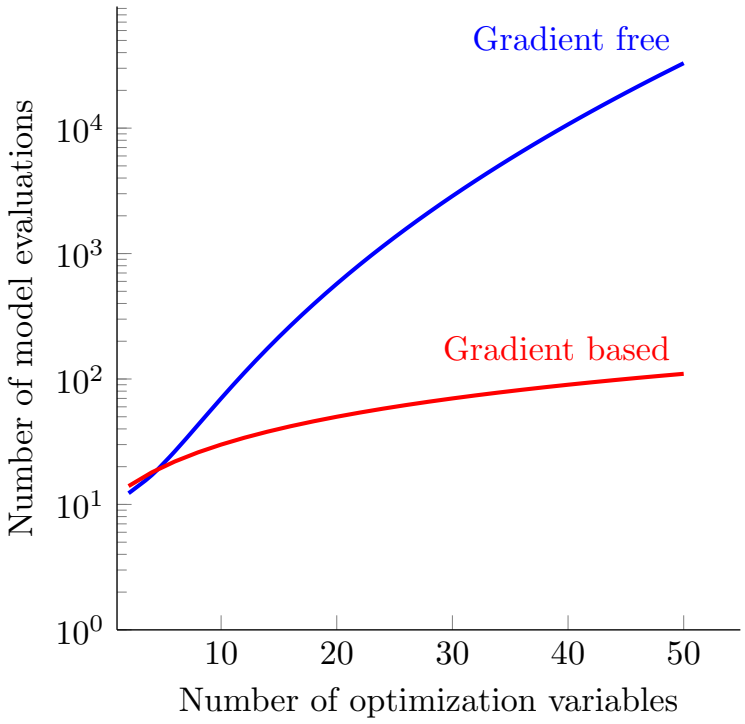

Fig. 8: **Scaling of required model evaluations with the number of optimization variables for GBOs and GFOs.** For GFOs, the number of evaluations grows super-polynomially, whereas GBOs scale approximately linearly, resulting in a difference of several orders of magnitude for high-dimensional problems. Reproduced from Martins et al. [95].

Second, there are mathematically rigorous criteria for GBOs for when an optimal solution

has been reached, while the optimality criteria for GFOs are largely heuristic. For first-order methods such as gradient descent, convergence to a global minimum can be ensured when the objective is convex. Regarding constraints, constraint-handling methods exist for GBOs that restrict the search to feasible designs, while it is difficult to assess whether a design is feasible or not based solely on zero-order information [94].

Third, because of the robustness of optimization algorithms, GBOs tolerate sparse discontinuities. However, gradient-free methods may be the only option if the objective exhibits excessive numerical noise and discontinuities. Tolerance to discontinuities is a key advantage of GFOs over gradient methods [95]. The implementation of gradient methods also requires knowledge of gradient expressions or access to numerical differentiation tools. Consequently, implementing GBOs can be more complex than GFOs, particularly due to noise and numerical instability. Recent advances in automatic differentiation for modeling frameworks such as PDE solvers [113] and deep learning libraries have significantly improved the accessibility of GBOs.

Fourth, regarding multimodality, some GFOs employ global search strategies, making them a popular choice for multimodal problems. Not all GFOs, however, employ global search; some are local methods. Gradient methods can be adapted for global search using *multi-start* or *basin-hopping strategies* [95].

A subclass of GFOs, evolutionary algorithms, are particularly common in DGS optimization. In this process, a population of candidate designs is evolved by mimicking biological principles such as selection, mutation, and recombination. The most widely used examples are particle swarm optimization (PSO) and genetic algorithms (GAs). These two algorithms can also be found in the literature on DGS design engineering in connection with a surrogate model for the objective function [44, 102].

The following section provides a comprehensive literature review of these and other optimization strategies applied to the design and operation of DGSs. It categorizes contributions by optimization type, objective function complexity, and degree of integration with physical modeling.

5 Literature review

We review published optimization studies for thermo-hydraulic DGSs, organizing them according to a newly proposed classification scheme for simulation-optimization pipelines and listed in Table 1. To connect the literature with the previous discussion of an optimization problem (cf. Section 3–4), for each study we identified the primary optimization variables and the objective function. For the computational methodology, we identify the underlying simulation model (TH model) according to Sections 3.2.1–3.2.3. Where applicable, the employed optimizer (cf. Section 4.4) is also listed in Table 1.

We identify three major simulation-optimization pipeline classes. For each class, the flow of information during simulation and optimization is illustrated in Figure 9, with distinctly colored arrows for each class. The classes use basic building blocks indicated

Tab. 1: **Literature review of geothermal system design optimization studies.** The table is divided into three classes of optimization methods. **Model**: Underlying model type, **Controls**: Design variables, **Objective**: Objective function, **Optimization method**: Optimization algorithm used.

Author, Year	Model	Controls	Objective	Optimization method	Ref.
I. Scenario comparison					
Blöcher et al., 2015	numerical	injection well path	t^b	comparison	[28]
Kong et al., 2017	numerical	$d(\mathbf{x}^{in}, \mathbf{x}^{pr})$, ϕ	C^{add}	comparison	[18]
Jiang et al., 2019	numerical	$d(\mathbf{x}^{in}, \mathbf{x}^{pr})$, ϕ	T^{bh}	comparison	[114]
Willems et al., 2019	numerical	$d(\mathbf{x}^{in}, \mathbf{x}^{pr})$, q	LCOH, t^b, E^{net}	comparison	[30]
Chong et al., 2021	numerical	$\Gamma^{\star\star}$	T^{bh}, T^{wh}, CoP	comparison	[98]
Zhang et al., 2021	numerical	$d(\mathbf{x}^{in}, \mathbf{x}^{pr})$, n_{in}, n_{pr}	T^{wh}, Δh	comparison	[101]
Ke et al., 2021	numerical	$d(\mathbf{x}^{in}, \mathbf{x}^{pr})$, ϕ	LCOH, R^g	comparison	[53]
Liu et al., 2022	numerical	$d(\mathbf{x}^{in}, \mathbf{x}^{pr})$	T^{wh}	comparison	[115]
Li et al., 2023	numerical	$d(\mathbf{x}^{in}, \mathbf{x}^{pr})$, ϕ	C^{add}, T^{wh}	comparison	[7]
Han et al., 2024	numerical	$d(\mathbf{x}^{in}, \mathbf{x}^{pr})$, q	R^g, t^b	comparison	[100]
Sun et al., 2024	numerical	$d(\mathbf{x}^{pr}, \mathbf{x}^{in})$, q, T^{in}	LCOH	comparison	[103]
Lei et al., 2025	numerical	$d(\mathbf{x}^{in}, \mathbf{x}^{pr})$, q	T^{wh}, W^{th}	comparison	[116]
II. Surrogate-based optimization					
Akin et al., 2010	FFNN	$\mathbf{x}^{in}$	T^{bh}, Δh	Exhaustive Search	[80]
Juliusson et al., 2013	M-ARX	q_i	NPV	Interior Point Method	[117]
Chen et al., 2015	MARS	$d(\mathbf{x}^{in}, \mathbf{x}^{pr})$	CCF	BOBYQA*	[106]

continued on next page

Table 1 – *continued from previous page*

Author, Year	**Model**	**Optimization Variables**	**Objective**	**Optimization Method**	**Ref.**
Schulte et al., 2020	ReLU, RSM	$\mathbf{x}^{pr}, \mathbf{x}^{in}$, p^{pump}	$E^{th}, \Delta p^{bh}$	PSO	[44]
Babaei et al., 2022	cubic RBF	$d(\mathbf{x}^{in}, \mathbf{x}^{pr})$, doublet spacing	CoP, R^g	LHS	[104]
Wang et al., 2022	RF	$d(\mathbf{x}^{in}, \mathbf{x}^{pr})$	$\mathrm{C}^{\mathrm{add}}$	GA	[102]
Ye et al., 2024	RSM	z^{in}, p^{pump}	I, W^{th}, C_{dr}	NSGA-II	[79]
Yan et al., 2024	FFNN	$d(\mathbf{x}^{in}, \mathbf{x}^{pr})$, T^{in}, q	E^{th}, T^{wh}	Adam	[54]
Li et al., 2025	LSTM-CNN	$\mathbf{x}^{in}$	$\mathrm{C}^{\mathrm{add}}$	GWO*	[83]
Sun et al., 2025	FFNN	q_i	T^{wh}	GA	[118]
Chen et al., 2025	CNN-GRU	q, T^{in}, $\mathbf{x}^{in}, \mathbf{x}^{pr}$	NPV	GA	[110]
		III. Direct optimization			
Gringarten et al., 1975	analytical	$d(\mathbf{x}^{in}, \mathbf{x}^{pr})$	T^{bh}	analytical solution	[29]
Tselepidou et al., 2010	analytical	$\mathbf{x}^{pr}$	$\mathrm{C}^{\mathrm{add}}$, C^{HG}	GA	[68]
Ansari et al., 2014	numerical	$\mathbf{x}^{in}, \mathbf{x}^{pr}$	E^{net}	PSO	[119]
Kahrobaei et al., 2019	numerical	$\mathbf{x}^{pr}, \mathbf{x}^{in}$	NPV	SSG	[109]
Blank et al., 2021	numerical	$\Gamma^{\star\star}$, $d(\mathbf{x}^{in}, \mathbf{x}^{pr})$, ϕ	E^{net}	DIRECT-L	[22]

***Acronyms used:** BOBYQA, Bounded Optimization by Quadratic Approximation; GWO, Grey-Wolf Optimizer; LHS, Latin-Hypercube Sampling

****Other notational remarks:** Γ refers to well grid parameters (cf. Section 4.1) where the exact choice of optimization parameters depends on the study; ϕ represents the orientation angle against the natural flow field.

by circles in the figure, including the underlying simulation model, the surrogate for the objective function, and an optimizer. All simulation-optimization pipelines take subsurface material parameters and optimization variables as input. When the workflow is executed, the optimal design is computed in the last step, where the notion of optimality depends on the method. To describe each class in detail, a more detailed description of the method and relevant articles for each of the three classes follows.

Scenario comparison (Class I, blue arrows) is the simplest approach, and it does not use mathematical optimizers; it relies only on the descriptive comparison of simulation results. First, a fixed batch of optimization variables $\mathbf{D} = (\mathbf{d}_1, \ldots, \mathbf{d}_N)$ is chosen. For each $\mathbf{d}_i$, the simulation model $\mathcal{M}$ for the DGS specified by design and operation conditions in this batch is evaluated. Then the computed state variables $\mathbf{S} = (\mathbf{s}_1, \ldots, \mathbf{s}_n) = (\mathcal{M}(\mathbf{d}_1), \ldots, \mathcal{M}(\mathbf{d}_N))$ are used to evaluate the objective function $\boldsymbol{\mathcal{F}}(\mathbf{S}) = \mathcal{F}(\mathbf{s}_1), \ldots, \mathcal{F}(\mathbf{s}_N)$. Finally, the design corresponding to the best objective function value is selected.

The surrogate-based optimization pipeline (Class II, yellow arrows) utilizes data generated by the simulation model $\mathcal{M}$ to train a surrogate model $\tilde{\mathcal{M}}$ for the objective function. Again, a batch of values for the optimization variables $\mathbf{D}$ is evaluated through the simulation model. The corresponding simulation results, i.e., state variables $\mathbf{S}$ are used to compute the objectives $\mathcal{F}(\mathcal{M}(\mathbf{D})) = \mathcal{F}(\mathbf{s}_1), \ldots, \mathcal{F}(\mathbf{s}_N)$. These results serve as training data for $\tilde{\mathcal{F}}$. Then $\tilde{\mathcal{F}}$ directly maps the design variables to the objective function, avoiding the direct evaluation of $\mathcal{M}$. Depending on the model type, the optimized design and operation variables can either be derived analytically or via coupling of $\tilde{\mathcal{F}}$ with a generic optimizer.

Indicated by red arrows in Figure 9, in Class III, the optimizer is directly supplied with the state variable of the respective optimization step $\mathbf{s}_n = \mathcal{M}(\mathbf{d}_n)$ from the underlying simulation model. Then the objective $\mathcal{F}(\mathbf{s}_n)$ and potentially derivatives with respect to the optimization variables are evaluated. Afterward, information is used to update the optimization variables $\mathbf{d}_{n+1}$ according to the optimization algorithm. Repeating this process until convergence yields the optimal design or operation.

5.1 Class I: Scenario comparison method

A defining feature of publications in Class I is the absence of systematic data postprocessing. Often, the results are simply plotted or tabulated, and the best design and operating conditions are identified. Sometimes only a few designs are compared, as in Blöcher et al. [28]. They used a complex three-dimensional TH model of the aquifer to compare the productivity index and production temperatures of three injection well paths.

Other articles compare multiple scenarios more systematically, analyzing trends across individual optimization variables. Kong et al. [18] investigated the effect of well spacing on additional costs due to thermal and hydraulic losses. Using this approach, both single systems [7, 100] and entire doublet fields [30, 53, 115] have been optimized.

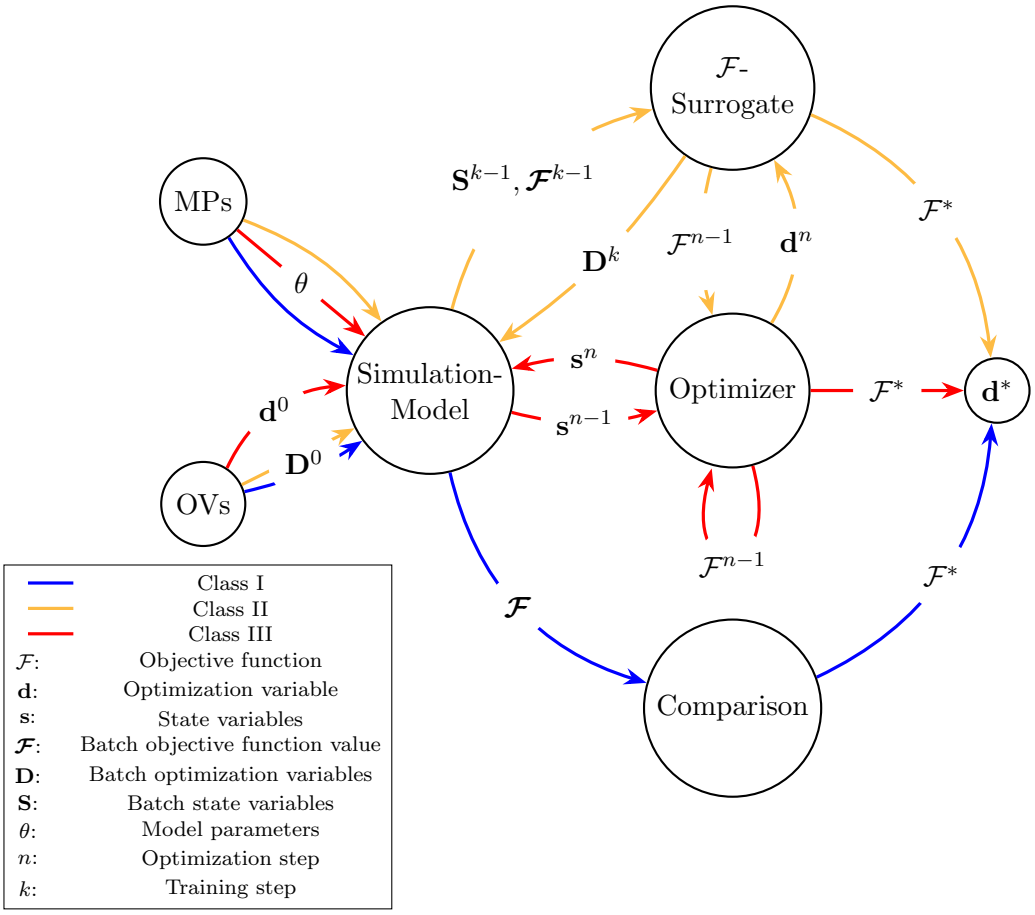

Fig. 9: **Flow chart for information of different simulation-optimization pipelines.** The figure shows the three newly proposed classification groups of existing simulation-optimization frameworks. The arrows indicate the direction of the data flow between the components. The common starting point of all methods are the model parameters (MPs) and initial optimization variables (OVs) for the TH simulation model. The blue arrows represent comparison based optimization, while the orange and red arrows indicate the surrogate-based and direct optimization method respectively. For the former classes, the iteration of optimization variables is driven by an optimizer, either directly coupled to the simulation model—evaluating the objective function internally—or to a surrogate model for the objective function. In general, the updating the optimization variables (n) does not coincide with the update of the surrogate model (k). If the approach succeeds, all methods arrive at optimal function values $\mathcal{F}^*$ and optimization variables d^*.

Chong et al. [98] evaluated a doublet and a five-well layout to maximize the system's energy efficiency with varying flow rates.

Jiang et al. [114] compared bottom-hole temperatures across various well placement strategies in a synthetic geothermal reservoir modelled with FEFLOW. They analysed the temperature distribution in a 2D vertical cross-section of a synthetic aquifer under different natural flow regimes. Subsequently, they evaluated the bottom-hole temperature of a steadily operating doublet system with various well distances and orientations relative to the natural flow direction. They concluded with recommendations for well placement and depth for aquifers with strong vertical flow, strong horizontal flow, and very weak natural flow.

5.2 Class II: Surrogate-based optimization

Akin et al. [80] proposed a brute-force optimization method coupled with an FFNN surrogate. The FFNN is trained on numerical simulations to predict the well pressures and temperatures from well coordinates, flow rates, and reinjection temperature. In view of the small number of parameters, the advantage of an ANN over other non-parametric modeling techniques remains unclear. Subsequently, they implemented an exhaustive search (brute-force) to select the well location with minimal temperature decline and depressurization.

Evolutionary algorithms are the primary choice in the publications belonging to Class II. Wang et al. [102] used a random forest (RF) model to model additional costs due to hydraulic head drawdown and temperature decline. They then used a GA to minimize these costs by optimizing the injection well position in their Dezhou geothermal field model. Ye et al. [79] conducted an MOO of a deep geothermal doublet in a fault-based geothermal system. The authors used the Non-dominated Sorting GA (NSGA-II) to optimize the drilling costs, thermal energy output, and the reservoir impedance simultaneously. The underlying surrogates were RSMs that predicted the objectives from a number of geological, design, and operation parameters. These included the depth of the injection and production wells and the pumping pressure.

Juliusson and Horne [117] studied a fractured reservoir model. The authors introduced an analytical formula (M-ARX) for the temporal temperature evolution of the production wells. The MPs were fitted to numerical simulation data. Subsequently, they optimized the injection rate distribution $(q_i^{in})_{i\in\{1,2,3,4\}}$ using an interior point method. The objective was to maximize the NPV of the system over 30 years.

Several researchers incorporated geological uncertainty into the optimization. Schulte et al. [44] optimized the placement and operation of six injector-producer doublets, considering geological uncertainty. The authors fitted a piecewise linear function for the time evolution of bottom-hole pressure and outlet temperature. They conducted this proxy-model fitting for each of 18 different major geological scenarios with data generated from numerical simulations. Subsequently, the authors used an RSM to predict T and p for interpolated optimization variables. The mean net thermal energy produced by

a design could then be predicted as the mean of the geological scenarios with proxy-model parameters generated by the RSM. Subsequently, they conducted multi-objective PSO (MOPSO) to find the best thermal energy output for different geological scenarios. Additionally, 18 GPR models were fitted, each modeling the uncertainties of a single scenario due to measurement uncertainties.

Babaei et al. [104] also took uncertainty into account by considering different fluvial channel ensembles in a synthetic 2D aquifer. Specifically, they quantified the averaged impact of preferential flowpaths on the CoP of the DGS via TH-simulations with different inhomogeneous permeability distributions. They used cubic RBF surrogates underlying the optimization and optimised the location of two injection and production wells using a candidate point strategy and Latin hypercube sampling. Their objectives were to maximize R^g and CoP.

Yan et al. [54] used a fundamentally different optimization approach. They coupled a forward neural network with an optimization network that determined a geothermal system's well control and design parameters. The forward model was a PINN that predicted the parameters of an analytical temperature model based on the rock's material properties and the design variables. The model was trained on high-fidelity simulation data for which the corresponding analytical MPs were determined via standard regression. The coupled control network received geological uncertainty parameters and computed the best design, either maximizing E^{th} or avoiding thermal breakthrough. The training of the control network followed an unsupervised training regime where the Adam optimizer was used to minimize a loss function encoding the objectives above and additional engineering constraints.

In a recent study, Chen et al. [110] optimize a doublet system in a fractured aquifer using a hybrid GRU-CNN together with a GA optimizer. The surrogate is trained on numerical simulations with homogeneous bulk permeability and spatially heterogeneous fracture aperture sampled from a log-normal random field. Additionally, the optimization variables — injection temperature, flow rate, and well placement parameters — are sampled uniformly in the training. The framework takes uncertainty into account by stochastic and risk-averse optimization under uncertain fracture apertures. Ultimately, the authors compare their different approaches and discuss limitations of the study.

5.3 Class III: Direct optimization methods

The literature in Class III is comparably sparse. Ansari et al. [119] studied a discrete ODP in a conference paper. The authors placed four injection and four production wells at the locations of 11 abandoned wells in the Gueydan geothermal field in Louisiana, USA. The selection was optimized using a PSO algorithm to maximize the net energy output E_{net} of a flash steam power plant.

Kahrobaei et al. [109] presented a method for optimal well placement using Stochastic Simplex Gradients (SSG). During an iteration, SSG samples optimization variables in the neighbourhood of the current iterate. The acquired data is subsequently used to

compute approximate gradients of $\mathcal{F}$ via linear regression. In their application, the authors maximized the NPV for computer-generated homogeneous and inhomogeneous 2D and 3D models.

Blank et al. [22] described an optimization of different well layouts in a 2D numerical model using the gradient-free DIRECT-L optimizer. The aquifer model was comparably simple, consisting of two permeability regions describing a fault zone and its surroundings. The aim was to optimize the well spacing and orientation of a checkerboard layout of 16 wells and a hexagonal arrangement. As an objective, they maximized the produced E^{th} during the operational lifetime. Their optimization was terminated after 50 steps unless the termination criteria were met earlier.

Tselepidou et al. [68] presented a study coupling an analytical hydraulic head expression with an optimizer. They optimized the placement of hydrothermal production wells to minimize C^{add} and pipe network costs, using an analytical expression for the hydraulic head. The aquifer was assumed to have two hydraulic conductivity regions. A pipe network connected the geothermal wells to a hot water storage area at the domain's boundary. The costs due to hydraulic head drawdown and network construction were then minimized using a GA.

5.4 Comparison of methods

The three classes are compared below with respect to their general features and computational costs. The methods surveyed in Table 1 are ranked qualitatively in Figure 10 by the computational cost of one optimization step and the number of optimization steps.

The publications in Class I almost exclusively use a few evaluations of numerical models to compare objective values. The authors primarily focus on accurate numerical aquifer models, making each simulation computationally demanding. Therefore, the publications in this class are primarily found in the lower right corner of Figure 10. Notably, simultaneous optimization of multiple DGSs via scenario comparison likely yields suboptimal results. Due to its simplicity, this approach is invaluable as a source of first approximations of optimal design and operation conditions. The results are a good starting point for a more detailed exploration of the objective function. Application of elementary data analysis can significantly improve the understanding of the objective function and yield better design decisions. Furthermore, the large number of simulations conducted in some Class I studies provides a basis for exploratory data analysis and, subsequently, for training surrogate models as in Class II, enabling a deeper exploration of optimal design and operation conditions.

This naturally motivates Class II: the computational efficiency of surrogate models allows the objective function to be evaluated rapidly, enabling more function evaluations at lower cost per step and thereby making GFOs such as evolutionary algorithms a viable choice.

The primary challenge of this approach is the generation of training data, for which the

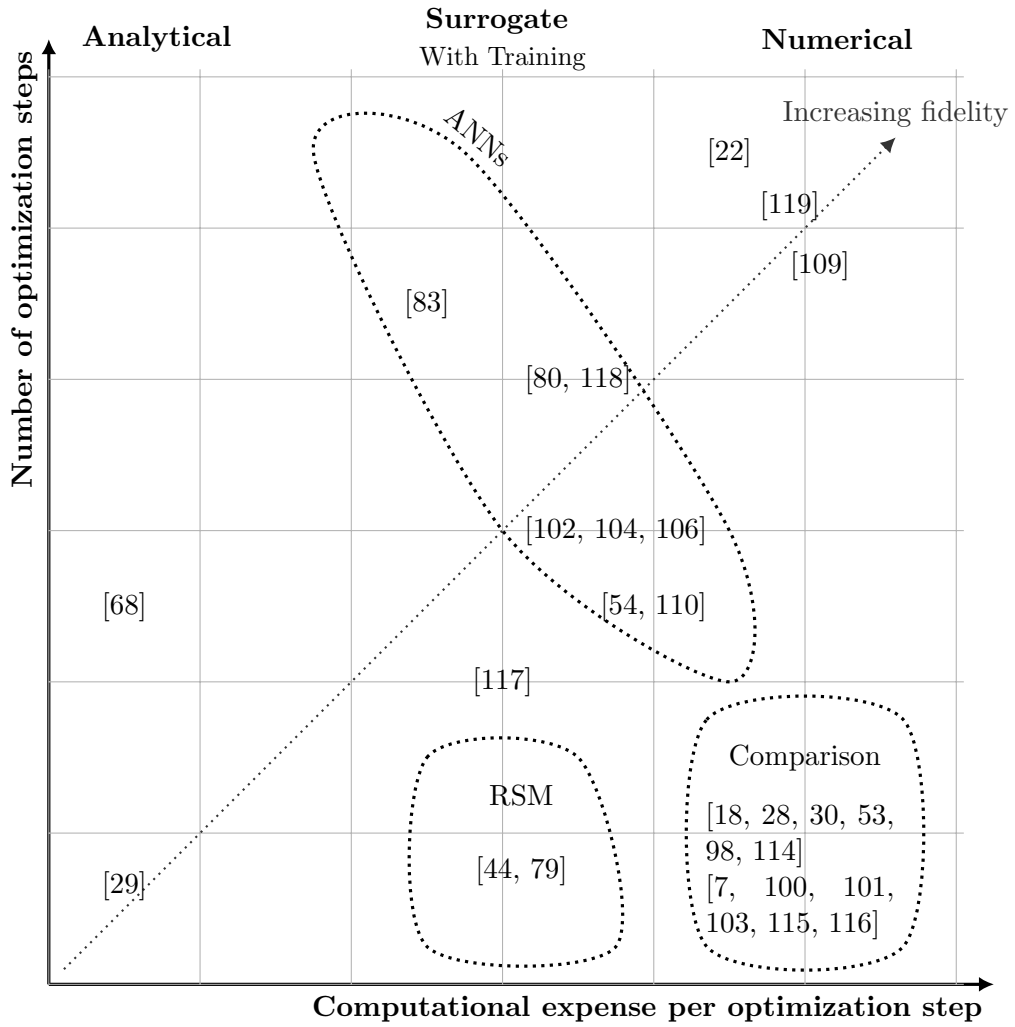

Fig. 10: **Qualitative comparison of the computational cost of different DGS optimization pipelines.** The cost of each pipeline is estimated as the product of the computational cost per optimization step and the total number of optimization steps. The publications are grouped into clusters of studies that employ the same method to model the objective function.

model types described in Section 3 are, in principle, available. However, in the extant literature, the data used to train the surrogates are almost exclusively generated by numerical simulations. Therefore, this method's primary computational demand lies in training the surrogate model. This also defines the appropriate use case for surrogate models: if the objective is smooth and well-behaved, direct coupling may be equally effective; if it is complex, a substantially larger training dataset is required to achieve sufficient surrogate accuracy. If the combined costs for data generation and optimization exceed those of a direct optimization pipeline, there is no methodological advantage. If, however, a surrogate approximates the objective with sufficient accuracy, the optimization can significantly benefit from its use. In comparison to Class I, surrogate-based optimization usually demands higher effort in implementation, often requiring data exchange between different software or modeling and optimization frameworks.

Class III uses the classical simulation-optimization approach and has the soundest theoretical foundation among the three classes. The principal advantage is that accuracy is not compromised by intermediary surrogates. In particular, the accuracy of the optimization result depends solely on the mathematical formulation of the optimization problem. Since the TH model is evaluated at every step, there are no interpolation errors of the kind introduced by surrogates in Class II. A further advantage is the *interpretability of results*. Since no surrogates are included, the optimization results can be traced directly to the underlying physical phenomena.

The computational cost of the underlying models limits the optimization. Very complex or large, highly resolved numerical TH models pose prohibitively high computational cost, particularly for GFOs. While GBOs, such as the adjoint method for PDE-constrained optimization, perform better, the required mathematics and implementation effort are non-trivial. As a result, corresponding optimization problems must be formulated carefully. Coupling simple numerical TH models with GFOs, as demonstrated by Blank et al. [22], offers a more accessible alternative without the need to compute gradients. Additionally, the accuracy of Class III results remains subject to uncertainties in the underlying TH model, a challenge discussed further in Section 6.

6 Challenges and Outlook

This section outlines some challenges and open research questions in deep geothermal system optimization. The open problems may be described as a triad of data scarcity, data uncertainty, and computational cost of the underlying numerical models. These problems can significantly impair the validity of optimization results and developing methods to address these challenges remains an open research question.

Data scarcity is a well-known challenge in geothermal system design optimization. Subsurface geological data are challenging to acquire and often available only at coarse resolution. While the data scarcity cannot be resolved theoretically, the impact of subsurface data uncertainty on the optimization process can be quantified. This requires building a reliable numerical model of the aquifer and the geothermal system together with a

method that propagates input data uncertainty through to the optimization output. Because of data uncertainty, robust optimization frameworks that explicitly account for parameter uncertainty, measurement noise, and model errors have been developed for other engineering applications. Approaches such as stochastic optimization, Bayesian optimization [120, 121], and uncertainty quantification [122] are promising but remain underexplored in geothermal system design.

To address the high computational cost of numerical models, high-quality surrogate models offer a promising avenue. In particular, recent advances in machine learning, such as PINNs, have been applied in geosciences [123]. However, these approaches remain underexplored in the context of geothermal design optimization.

Further potential for improvement lies in the choice of optimization algorithm. As discussed in Section 5, the few studies that directly couple optimization algorithms with TH models employ GFOs. Methods such as GA, PSO, and exhaustive search are most commonly used. While flexible and straightforward to implement, they scale poorly with problem complexity. Advances in automatic differentiation and the adjoint method are making gradient-based optimizers increasingly viable.

Studies on shallow groundwater heat pumps and tidal power farms have demonstrated that gradient-based optimizers can be applied successfully to complex PDE models [124, 125]. To the best of our knowledge, their application in DGS design and operation optimization has not been reported. While using GBOs is a promising approach, it demands considerable expertise in numerical modeling and optimization. Current implementations of PDE-constrained optimization (PDECO) via the adjoint approach remain inaccessible to non-experts. Therefore, developing user-friendly software packages handling most of the complexities internally would represent a significant step forward.

An important aspect of design optimization is the formulation of the optimization problem itself — that is, the choice of design variables and objective function. Jointly optimizing multiple DGSs within district heating grid planning could improve both project economics and social welfare [3]. In this research direction, fast analytical models could in particular serve as invaluable tools, as shown by research on groundwater heat pumps [33, 126].

Finally, all optimization approaches lack standardized benchmark scenarios and validation methods. The development of such test cases would significantly facilitate the evaluation of different optimization approaches and enable a comprehensible performance comparison for non-experts.

7 Conclusion

This review provides an overview of the integration of mathematical optimization techniques with the modeling and design of conventional deep geothermal systems (DGS). In doing so, it serves as a comprehensive reference for researchers and practitioners

interested in the systematic improvement of geothermal system performance through optimization.

The review systematically addresses the formulation of the underlying TH models and DGS optimization problems. It identifies common design and control variables such as well placement, flow rates, and reinjection temperatures. The structure of objective functions—ranging from thermal energy output and reservoir impedance to economic indicators like the net present value (NPV) and the levelized cost of energy (LCOE)—is discussed in detail. Gradient-based and gradient-free algorithms are evaluated in terms of scalability, constraint handling, and applicability to different model types. Particular attention is given to evolutionary algorithms and surrogate-based methods, which are prevalent in the reviewed literature.

The review proposes a three-class classification based on the degree of integration between simulation and optimization: scenario comparison, surrogate-based optimization, and direct simulation-optimization coupling. Each class is illustrated with representative studies, highlighting both methodological trends and gaps.

The review identifies several challenges for future research: (i) the limited use of advanced gradient-based optimization despite its superior scaling; (ii) underexplored potential of multi-fidelity and reduced-order models; (iii) insufficient treatment of uncertainty and robustness in optimization outcomes; and (iv) the lack of standardized benchmarks and validation frameworks in the field.

Addressing these issues through continued methodological development and broader adoption of simulation-optimization frameworks will be essential for realizing the full potential of DGS in the global energy transition.

Tab. 2: Notation of physical and mathematical entities

Symbol	Name	Type	SI-Unit
	Modeling		
h	hydraulic head	state variable	m
Δh	hydraulic head drawdown	state variable	m
p	pressure	state variable	Pa
$\mathbf{q}$	Darcy velocity	state variable	m/s
Q^f	combined volumetric source	scalar function	m^3/s
Q^t	combined heat source	scalar function	W/m^3
S	storativity coefficient	constant scalar	–
T	temperature field	state variable	K
T^{wh}	wellhead temperature	state variable	K
T^{bh}	bottom hole temperature	state variable	K
LT	system life time	constant scalar	a
i	interest rate	constant scalar	–
C^e	price per energy unit	constant scalar	\$/J
CF	cash flow	scalar function	\$
	Material properties		
ϵ	porosity	constant scalar	–
$\mathbf{K}$	permeability	constant tensor	m^2
$\mathbf{D}_{\text{mech}}$	mechanical dispersion tensor	constant tensor	m/s
τ	transmissivity	constant scalar	m^2/s
$\mathbf{\Lambda}$	thermal dispersion tensor	constant tensor	$J/m \cdot s \cdot K$
ρ^f	density of water	constant scalar	kg/m^3
ρ^s	density of solid	constant scalar	kg/m^3
c^f	heat capacity of water	constant scalar	$J/kg \cdot K$
c^s	heat capacity of solid	constant scalar	$J/kg \cdot K$
μ	dynamic viscosity	scalar function	$Pa \cdot s$
Ω	aquifer region	2/3-dim set	-
η_L	longitudinal dispersivity	constant scalar	m
η_T	transversal dispersivity	constant scalar	m
λ^f	fluid thermal conductivity	constant scalar	$J/m \cdot s \cdot K$
λ^s	solid thermal conductivity	constant scalar	$J/m \cdot s \cdot K$
$\mathbf{g}$	gravitational acceleration	constant vector	m/s^2
	Optimization		
n_{in}, n_{pr}	number of injection/production wells	design variable	–
$\mathbf{x}^{in}$	position of injection well	design variable	(m,m,m)
$\mathbf{x}^{pr}$	position of production well	design variable	(m,m,m)
$d(\mathbf{x}^{in}, \mathbf{x}^{pr})$	well spacing	design variable	m

q	volumetric flow rate	control variable	m^3/s
p^{pump}	pumping pressure	control variable	Pa
T^{in}	temperature of injected water	control variable	K
t^b	thermal breakthrough time	objective function	s
R^g	recovery factor	objective function	–
CoP	coefficient of performance	objective function	–
C_{dr}	drilling cost	objective function	\$
LCOE	levelized cost of energy	objective function	$\$ /J$
E^{net}	net produced energy	objective function	J
E^{el}	produced electrical energy	objective function	J
W^{th}	instantaneous thermal power	objective function	W
E^{th}	produced thermal energy	objective function	J
E^{pump}	pump energy consumption	objective function	J
C^{CAPEX}	total capital expenditure	objective function	\$
C^{OPEX}	operation and maintenance expenditure	objective function	\$
C^{HG}	network construction cost	objective function	\$
C^{add}	additional costs	objective function	\$
NPV	net present value	objective function	\$
CCF	cumulated cash flow	objective function	\$

Funding

This work is partially funded by the Bavarian Ministry of Economic Affairs and by the Bavarian Environment Agency through the Project BeM-TG.

Declarations

Ethics approval The manuscript complies with the ethical standards of the journal.

Consent to participate Not applicable.

Competing interests The authors declare that they have no known competing financial interests or personal relationships that could have appeared to influence the work reported in this paper.

References

[1] Lund, J. W., Huttrer, G. W., and Toth, A. N. "Characteristics and Trends in Geothermal Development and Use, 1995 to 2020". In: *Geothermics* 105 (2022), p. 102522.

[2] Werner, S. "International Review of District Heating and Cooling". In: *Energy* 137 (2017), pp. 617–631.

[3] Molar-Cruz, A. et al. "Techno-Economic Optimization of Large-Scale Deep Geothermal District Heating Systems with Long-Distance Heat Transport". In: *Energy Convers. Manage.* 267 (2022), p. 115906.

[4] Kavvadias, K. C. and Quoilin, S. "Exploiting Waste Heat Potential by Long Distance Heat Transmission: Design Considerations and Techno-Economic Assessment". In: *Appl. Energy* 216 (2018), pp. 452–465.

[5] Lopez, S. et al. "40 Years of Dogger Aquifer Management in Ile-de-France, Paris Basin, France". In: *Geothermics*. Special Issue on the Sustainable Utilization of Geothermal Energy 39.4 (2010), pp. 339–356.

[6] Dussel, M. et al. "Forecast for Thermal Water Use from Upper Jurassic Carbonates in the Munich Region (South German Molasse Basin)". In: *Geothermics* 60 (2016), pp. 13–30.

[7] Li, S. et al. "Numerical Optimization of Geothermal Energy Extraction from Deep Karst Reservoir in North China". In: *Renew. Energy* 202 (2023), pp. 1071–1085.

[8] M. Bauer et al., eds. *Handbuch Tiefe Geothermie: Prospektion, Exploration, Realisierung, Nutzung*. Berlin, Heidelberg: Springer, 2014.

[9] Torresan, F. et al. "Numerical Modeling as a Tool for Evaluating the Renewability of Geothermal Resources: The Case Study of the Euganean Geothermal System (NE Italy)". In: *Environ. Geochem. Health* 44.7 (7 2022), pp. 2135–2162.

[10] Shinn, J. H. et al. *Investigation of Ecosystems Impacts from Geothermal Development in Imperial Valley, California*. California Univ., Livermore (USA). Lawrence Livermore Lab., 1979. URL: https://www.osti.gov/biblio/6078278.

[11] Birkle, P. and Merkel, B. "Environmental Impact by Spill of Geothermal Fluids at the Geothermal Field of Los Azufres, Michoacán, Mexico". In: *Water, Air, Soil Pollut.* 124.3 (2000), pp. 371–410.

[12] Balaban, T. Ö., Bülbül, A., and Tarcan, G. "Review of Water and Soil Contamination in and around Salihli Geothermal Field (Manisa, Turkey)". In: *Arabian J. Geosci.* 10.23 (2017), pp. 523–542.

[13] Kaya, E., Zarrouk, S. J., and O'Sullivan, M. J. "Reinjection in Geothermal Fields: A Review of Worldwide Experience". In: *Renew. Sustain. Energy Rev.* 15.1 (2011), pp. 47–68.

[14] Kamila, Z., Kaya, E., and Zarrouk, S. J. "Reinjection in Geothermal Fields: An Updated Worldwide Review 2020". In: *Geothermics* 89 (2021), p. 101970.

[15] Stefansson, V.-đ. "Geothermal Reinjection Experience". In: *Geothermics* 26.1 (1997), pp. 99–139.

[16] Rivera Diaz, A., Kaya, E., and Zarrouk, S. J. "Reinjection in Geothermal Fields - a Worldwide Review Update". In: *Renew. Sustain. Energy Rev.* 53 (2016), pp. 105–162.

[17] Swyer, M. W. et al. "New Injection Strategies at Blue Mountain, Nevada through Tracer Test Analysis, Injection-Production Correlation, and an Improved Conceptual Model". In: *Proceedings of 41st Workshop on Geothermal Reservoir Engineering*. 2016, pp. 22–24. URL: https://altarockenergy.com/wp-content/uploads/2013/06/Swyer-et-al.-2016.pdf.

[18] Kong, Y. et al. "Optimization of Well-Doublet Placement in Geothermal Reservoirs Using Numerical Simulation and Economic Analysis". In: *Environ. Earth Sci.* 76.3 (2017), pp. 118–124.

[19] Willems, C. J. L. et al. "An Evaluation of Interferences in Heat Production from Low Enthalpy Geothermal Doublets Systems". In: *Energy* 135 (2017), pp. 500–512.

[20] *UmweltAtlas Bayern - LfU Bayern*. URL: https://www.lfu.bayern.de/umweltdaten/kartendienste/umweltatlas/index.htm.

[21] Vörös, R. et al. "Thermal Modelling of Long Term Circulation of Multi-Well Development at the Cooper Basin Hot Fractured Rock (HFR) Project and Current Proposed Scale-up Program". In: *Proceedings of the 32nd Workshop on Geothermal Reservoir Engineering*. 2007. URL: https://pangea.stanford.edu/ERE/pdf/IGAstandard/SGW/2007/voros.pdf.

[22] Blank, L. et al. "Modeling, Simulation, and Optimization of Geothermal Energy Production from Hot Sedimentary Aquifers". In: *Comput. Geosci.* 25.1 (2021), pp. 67–104.

[23] Mantei, N., Rioseco, E. M., and Moeck, I. S. *3D Numerical Study of Geothermal Reservoir Performance of Homogeneous Sectors of Mesozoic Sandstone Formations in the North German Basin Developed by Smart Multi-Well Systems*. 2024. Pre-published.

[24] Schölderle, F. et al. "Monitoring Cold Water Injections for Reservoir Characterization Using a Permanent Fiber Optic Installation in a Geothermal Production Well in the Southern German Molasse Basin". In: *Geotherm. Energy* 9.1 (2021), pp. 21–56.

[25] Franco, A. and Vaccaro, M. "Numerical Simulation of Geothermal Reservoirs for the Sustainable Design of Energy Plants: A Review". In: *Renew. Sustain. Energy Rev.* 30 (2014), pp. 987–1002.

[26] Pandey, S. N., Vishal, V., and Chaudhuri, A. "Geothermal Reservoir Modeling in a Coupled Thermo-Hydro-Mechanical-Chemical Approach: A Review". In: *Earth Sci. Rev.* 185 (2018), pp. 1157–1169.

[27] Gunnarsson, G. and Aradóttir, E. S. P. "The Deep Roots of Geothermal Systems in Volcanic Areas: Boundary Conditions and Heat Sources in Reservoir Modeling". In: *Transp. Porous Media* 108.1 (2015), pp. 43–59.

[28] Blöcher, G. et al. "Evaluation of Three Exploitation Concepts for a Deep Geothermal System in the North German Basin". In: *Comput. Geosci.* 82 (2015), pp. 120–129.

[29] Gringarten, A. C. and Sauty, J. P. "A Theoretical Study of Heat Extraction from Aquifers with Uniform Regional Flow". In: *Journal of Geophysical Research* 80 (1975), pp. 4956–4962.

[30] Willems, C. J. L. and M. Nick, H. "Towards Optimisation of Geothermal Heat Recovery: An Example from the West Netherlands Basin". In: *Appl. Energy* 247 (2019), pp. 582–593.

[31] Rajabi, M. M. and Chen, M. "Simulation-Optimization with Machine Learning for Geothermal Reservoir Recovery: Current Status and Future Prospects". In: *Adv. Geo-Energy Res.* 6.6 (6 2022), pp. 451–453.

[32] Özkaraca, O. "A Review on Usage of Optimization Methods in Geothermal Power Generation". In: *Mugla J. Sci. Technol.* 4.1 (1 2018), pp. 130–136.

[33] Halilovic, S. et al. "Optimization Approaches for the Design and Operation of Open-Loop Shallow Geothermal Systems". In: *Advances in Geosciences*. European Geosciences Union General Assembly 2023, EGU Division Energy, Resources & Environment (ERE) - EGU General Assembly 2023, Vienna, Austria, 23–28 April 2023. Vol. 62. Copernicus GmbH, 2023, pp. 57–66.

[34] Sanyal, S. K. "Classification of Geothermal Systems–a Possible Scheme". In: *Thirtieth Workshop on Geothermal Reservoir Engineering*. Vol. 2. 02. Stanford University Stanford, California, 2005. URL: `http://pangea.stanford.edu/ERE/pdf/IGAstandard/SGW/2005/sanyal1.pdf`.

[35] Moeck, I. S. “Catalog of Geothermal Play Types Based on Geologic Controls”. In: *Renew. Sustain. Energy Rev.* 37 (2014), pp. 867–882.

[36] Khodayar, M. and Björnsson, S. “Conventional Geothermal Systems and Unconventional Geothermal Developments: An Overview”. In: *OPEN J. Geol.* 14.2 (2 2024), pp. 196–246.

[37] Chen, B. et al. “A Review of Hydraulic Fracturing Simulation”. In: *Arch. Comput. Methods Eng.* 29.4 (2022), pp. 1–58.

[38] Li, S., Wang, S., and Tang, H. “Stimulation Mechanism and Design of Enhanced Geothermal Systems: A Comprehensive Review”. In: *Renew. Sustain. Energy Rev.* 155 (2022), p. 111914.

[39] Lukawski, M. Z., Silverman, R. L., and Tester, J. W. “Uncertainty Analysis of Geothermal Well Drilling and Completion Costs”. In: *Geothermics* 64 (2016), pp. 382–391.

[40] Beckers, K. F. et al. “Evaluating the Feasibility of Geothermal Deep Direct-Use in the United States”. In: *Energy Convers. Manage.* 243 (2021), p. 114335.

[41] Hackstein, F. V. and Madlener, R. “Sustainable Operation of Geothermal Power Plants: Why Economics Matters”. In: *Geotherm. Energy* 9.1 (2021), pp. 10–39.

[42] Lund, J. W. and Toth, A. N. “Direct Utilization of Geothermal Energy 2020 Worldwide Review”. In: *Geothermics* 90 (2021), p. 101915.

[43] Sharmin, T. et al. “A State-of-the-Art Review on Geothermal Energy Extraction, Utilization, and Improvement Strategies: Conventional, Hybridized, and Enhanced Geothermal Systems”. In: *Int. J. Thermofluids* 18 (2023), p. 100323.

[44] Schulte, D. O. et al. “Multi-Objective Optimization under Uncertainty of Geothermal Reservoirs Using Experimental Design-Based Proxy Models”. In: *Geothermics* 86 (2020), p. 101792.

[45] Daniilidis, A., Alpsoy, B., and Herber, R. “Impact of Technical and Economic Uncertainties on the Economic Performance of a Deep Geothermal Heat System”. In: *Renew. Energy* 114 (2017), pp. 805–816.

[46] Fink, J., Heim, E., and Klitzsch, N. *State of the Art in Deep Geothermal Energy in Europe: With Focus on Direct Heating*. SpringerBriefs in Earth System Sciences. Cham: Springer International Publishing, 2022.

[47] Bundschuh, J. and A, M. C. S. *Introduction to the Numerical Modeling of Groundwater and Geothermal Systems: Fundamentals of Mass, Energy and Solute Transport in Poroelastic Rocks*. London: CRC Press, 2010. 522 pp.

[48] Diersch, H.-J. G. *FEFLOW: Finite Element Modeling of Flow, Mass and Heat Transport in Porous and Fractured Media*. Berlin, Heidelberg: Springer, 2014.

[49] Bear, J. *Dynamics of Fluids in Porous Media*. Courier Corporation, 1988. 806 pp.

[50] Bodvarsson, G., Pruess, K., and Lippmann, M. “Modeling of Geothermal Systems”. In: *J. Pet. Technol.* 38.9 (1986), pp. 1007–1021.

[51] Hughes, J. D., Langevin, C. D., and Banta, E. R. *Documentation for the MODFLOW 6 Framework*. 6-A57. U.S. Geological Survey, 2017.

[52] Naumov, D. et al. *OpenGeoSys*. Version 6.5.5. Zenodo, 2025.

[53] Ke, T. et al. "Study on Heat Extraction Performance of Multiple-Doublet System in Hot Sedimentary Aquifers: Case Study from the Xianyang Geothermal Field, Northwest China". In: *Geothermics* 94 (2021), p. 102131.

[54] Yan, B. et al. "Physics-Informed Machine Learning for Noniterative Optimization in Geothermal Energy Recovery". In: *Appl. Energy* 365 (2024), p. 123179.

[55] Tao, J. et al. "Coupled Thermo-Hydro-Mechanical-Chemical Modeling of Permeability Evolution in a CO2-circulated Geothermal Reservoir". In: *Geofluids* 2019.1 (2019), p. 5210730.

[56] Diersch, H. .-. G. and Kolditz, O. "Variable-Density Flow and Transport in Porous Media: Approaches and Challenges". In: *Adv. Water Resour.* 25.8 (2002), pp. 899–944.

[57] Saeid, S., Al-Khoury, R., and Barends, F. "An Efficient Computational Model for Deep Low-Enthalpy Geothermal Systems". In: *Comput. Geosci.* 51 (2013), pp. 400–409.

[58] Tian, X., Volkov, O., and Voskov, D. "An Advanced Inverse Modeling Framework for Efficient and Flexible Adjoint-Based History Matching of Geothermal Fields". In: *Geothermics* 116 (2024), p. 102849.

[59] Leeuwen, T. van and Herrmann, F. J. "A Penalty Method for PDE-constrained Optimization in Inverse Problems". In: *Inverse Probl.* 32.1 (2015), p. 015007.

[60] Sagar, B., Yakowitz, S., and Duckstein, L. "A Direct Method for the Identification of the Parameters of Dynamic Nonhomogeneous Aquifers". In: *Water Resour. Res.* 11.4 (1975), pp. 563–570.

[61] Grossmann, C., Roos, H.-G., and Stynes, M. *Numerical Treatment of Partial Differential Equations*. Berlin, Heidelberg: Springer, 2007.

[62] *Validation of ECLIPSE Reservoir Simulator for Geothermal Problems*. URL: `https://www.slb.com/resource-library/technical-paper/geothermal/validation-of-eclipse-reservoir-simulator-for-geothermal-problems`.

[63] Pruess, K., Oldenburg, C. M., and Moridis, G. J. *TOUGH2 User's Guide Version 2*. 1999. URL: `https://escholarship.org/content/qt4df6700h/qt4df6700h.pdf`.

[64] Pruess, K. "The TOUGH Codes—a Family of Simulation Tools for Multiphase Flow and Transport Processes in Permeable Media". In: *Vadose Zone J.* 3.3 (2004), pp. 738–746.

[65] Cacace, M. and Jacquey, A. B. "Flexible Parallel Implicit Modelling of Coupled Thermal–Hydraulic–Mechanical Processes in Fractured Rocks". In: *Solid Earth* 8.5 (2017), pp. 921–941.

[66] Carslaw, H. S. and Jaeger, J. C. *Conduction of Heat in Solids*. Clarendon Press, 1986. 524 pp.

[67] Theis, C. V. "The Relation between the Lowering of the Piezometric Surface and the Rate and Duration of Discharge of a Well Using Ground-Water Storage". In: *EOS Trans. Trans. Am. Geophys. Union* 16.2 (1935), pp. 519–524.

[68] Tselepidou, K. and Katsifarakis, K. L. "Optimization of the Exploitation System of a Low Enthalpy Geothermal Aquifer with Zones of Different Transmissivities and Temperatures". In: *Renew. Energy*. Special Section: IST National Conference 2009 35.7 (2010), pp. 1408–1413.

[69] Muskat, M. *The Flow of Homogeneous Fluids through Porous Media*. Vol. 46. McGraw-Hill Book Company, 1937.

[70] Lauwerier, H. A. "The Transport of Heat in an Oil Layer Caused by the Injection of Hot Fluid". In: *Appl. Sci. Res. Sect. a* 5.2 (1955), pp. 145–150.

[71] Bodvarsson, G. "Thermal Problems in the Siting of Reinjection Wells". In: *Geothermics* 1.2 (1972), pp. 63–66.

[72] Bodvarsson, G. S. and Tsang, C. F. "Injection and Thermal Breakthrough in Fractured Geothermal Reservoirs". In: *J. Geophys. Res.: Solid Earth* 87.B2 (1982), pp. 1031–1048.

[73] Kocabas, I. and Horne, R. N. "A New Method of Forecasting the Thermal Breakthrough Time during Reinjection in Geothermal Reservoirs". In: *Proceedings, 15th Workshop on Geothermal Reservoir Engineering*. 1990. URL: `http://pangea.stanford.edu/ERE/pdf/IGAstandard/SGW/1990/Kocabas.pdf`.

[74] Stopa, J. and Wojnarowski, P. "Analytical Model of Cold Water Front Movement in a Geothermal Reservoir". In: *Geothermics* 35.1 (2006), pp. 59–69.

[75] Birdsell, D. T. et al. "Analytical Solutions to Evaluate the Geothermal Energy Generation Potential from Sedimentary-Basin Reservoirs". In: *Geothermics* 116 (2024), p. 102843.

[76] Jiang, P., Zhou, Q., and Shao, X. *Surrogate Model-Based Engineering Design and Optimization*. Springer Tracts in Mechanical Engineering. Singapore: Springer, 2020.

[77] Asher, M. J. et al. "A Review of Surrogate Models and Their Application to Groundwater Modeling". In: *Water Resour. Res.* 51.8 (2015), pp. 5957–5973.

[78] Razavi, S., Tolson, B. A., and Burn, D. H. "Review of Surrogate Modeling in Water Resources". In: *Water Resour. Res.* 48.7 (2012), pp. 1–32.

[79] Ye, Z., Wang, J. G., and Yang, J. "A Multi-Objective Optimization Approach for a Fault Geothermal System Based on Response Surface Method". In: *Geothermics* 117 (2024), p. 102887.

[80] Akın, S., Kok, M. V., and Uraz, I. "Optimization of Well Placement Geothermal Reservoirs Using Artificial Intelligence". In: *Comput. Geosci.* 36.6 (2010), pp. 776–785.

[81] Delpisheh, M. et al. “Leveraging Machine Learning in Porous Media”. In: *J. Mater. Chem. A* 12.32 (2024), pp. 20717–20782.

[82] Shadab, M. A. et al. “Investigating Steady Unconfined Groundwater Flow Using Physics Informed Neural Networks”. In: *Adv. Water Resour.* 177 (2023), p. 104445.

[83] Li, F. et al. “A Surrogate Model-Based Optimization Approach for Geothermal Well-Doublet Placement Using a Regularized LSTM-CNN Model and Grey Wolf Optimizer”. In: *Sustainability* 17.1 (1 2025), pp. 266–296.

[84] Degen, D. et al. “Perspectives of Physics-Based Machine Learning Strategies for Geoscientific Applications Governed by Partial Differential Equations”. In: *Geosci. Model Dev.* 16.24 (2023), pp. 7375–7409.

[85] LeGresley, P. and Alonso, J. “Airfoil Design Optimization Using Reduced Order Models Based on Proper Orthogonal Decomposition”. In: *Fluids 2000 Conference and Exhibit*. Fluids 2000 Conference and Exhibit. Denver,CO,U.S.A.: American Institute of Aeronautics and Astronautics, 2000.

[86] He, X. et al. “Robust Aerodynamic Shape Optimization—from a Circle to an Airfoil”. In: *Aerosp. Sci. Technol.* 87 (2019), pp. 48–61.

[87] Lyu, Z., Kenway, G. K. W., and Martins, J. R. R. A. “Aerodynamic Shape Optimization Investigations of the Common Research Model Wing Benchmark”. In: *AIAA J.* 53.4 (2015), pp. 968–985.

[88] Xudong, W. et al. “Shape Optimization of Wind Turbine Blades”. In: *Wind Energy* 12.8 (2009), pp. 781–803.

[89] Schwenzer, M. et al. “Review on Model Predictive Control: An Engineering Perspective”. In: *Int. J. Adv. Manuf. Technol.* 117.5 (2021), pp. 1327–1349.

[90] Morari, M. and H. Lee, J. “Model Predictive Control: Past, Present and Future”. In: *Comput. Chem. Eng.* 23.4 (1999), pp. 667–682.

[91] Hu, Z., Gao, B., and Mao, Y. “Nonlinear Model Predictive Control-Based Active Power Dispatch Strategy for Wind Power Plant Considering Dynamic Wake Effect”. In: *Int. J. Electr. Power Energy Syst.* 148 (2023), p. 108996.

[92] Eliasi, H., Menhaj, M. B., and Davilu, H. “Robust Nonlinear Model Predictive Control for a PWR Nuclear Power Plant”. In: *Prog. Nucl. Energy* 54.1 (2012), pp. 177–185.

[93] Tanjavooru, V. T. et al. “Optimal Power Split Control for State of Charge Balancing in Battery Systems with Integrated Spatial Thermal Analysis and Aging Estimation”. In: *Energy Storage* 7.4 (2025), e70206.

[94] Boyd, S. and Vandenberghe, L. *Convex Optimization*. 1st ed. Cambridge University Press, 2004.

[95] Martins, J. R. R. A. and Ning, A. *Engineering Design Optimization*. 1st ed. Cambridge University Press, 2021.

[96] Amaran, S. et al. “Simulation Optimization: A Review of Algorithms and Applications”. In: *Ann. Oper. Res.* 240.1 (2016), pp. 351–380.

[97] Gosavi, A. *Simulation-Based Optimization: Parametric Optimization Techniques and Reinforcement Learning*. Boston, MA: Springer, 2014. 534 pp.

[98] Chong, Q., Wang, J., and Gates, I. D. “Evaluation of Energy Extraction from a Geothermal Resource in Central Alberta, Canada Using Different Well Configurations”. In: *Geothermics* 96 (2021), p. 102222.

[99] Gutiérrez-Negrín, L. C. A. “Evolution of Worldwide Geothermal Power 2020–2023”. In: *Geotherm. Energy* 12.1 (2024), pp. 14–73.

[100] Han, Y. et al. “Optimizing the Heat Extraction Performance in the Qingfeng Karst Geothermal Reservoir”. In: *Geoenergy Sci. Eng.* 243 (2024), p. 213378.

[101] Zhang, S. et al. “Well Placement Optimization for Large-Scale Geothermal Energy Exploitation Considering Nature Hydro-Thermal Processes in the Gonghe Basin, China”. In: *J. Cleaner Prod.* 317 (2021), p. 128391.

[102] Wang, J. et al. “A Robust Optimization Approach of Well Placement for Doublet in Heterogeneous Geothermal Reservoirs Using Random Forest Technique and Genetic Algorithm”. In: *Energy* 254 (2022), p. 124427.

[103] Sun, W. et al. “Qualitative Assessment of Optimizing the Well Spacings Based on the Economic Analysis”. In: *Geothermal Energy* 12.1 (2024), p. 16.

[104] Babaei, M. et al. “Optimisation of Heat Recovery from Low-Enthalpy Aquifers with Geological Uncertainty Using Surrogate Response Surfaces and Simple Search Algorithms”. In: *Sustainable Energy Technol. Assess.* 49 (2022), p. 101754.

[105] Willems, C. J. L. et al. “The Impact of Reduction of Doublet Well Spacing on the Net Present Value and the Life Time of Fluvial Hot Sedimentary Aquifer Doublets”. In: *Geothermics* 68 (2017), pp. 54–66.

[106] Chen, M. et al. “An Efficient Optimization of Well Placement and Control for a Geothermal Prospect under Geological Uncertainty”. In: *Appl. Energy* 137 (2015), pp. 352–363.

[107] Zweifel, P., Praktiknjo, A., and Erdmann, G. *Energy Economics*. Springer Texts in Business and Economics. Berlin, Heidelberg: Springer, 2017.

[108] Wees, J.-D. van et al. “Geothermal Aquifer Performance Assessment for Direct Heat Production – Methodology and Application to Rotliegend Aquifers”. In: *Neth. J. Geosci.* 91.4 (2012), pp. 651–665.

[109] Kahrobaei, S. et al. “Regional Scale Geothermal Field Development Optimization under Geological Uncertainties”. In: European Geothermal Congress 2019. The Hague, The Netherlands, 2019. URL: `https://eprints.gla.ac.uk/189689/`.

[110] Chen, J., Zhao, Z., and Wang, J. “A Time-Series Forecasting Model-Based Optimization Approach for Well-Doublet System in Geothermal Reservoirs under Geological Uncertainty”. In: *Energy* 330 (2025), p. 136926.

[111] Weber, C., Möst, D., and Fichtner, W. *Economics of Power Systems: Fundamentals for Sustainable Energy*. Springer Texts in Business and Economics. Cham: Springer International Publishing, 2022.

[112] L. Qi, K. Teo, and X. Yang, eds. *Optimization and Control with Applications*. Applied Optimization. Boston, MA: Springer US, 2005.

[113] Funke, S. W. and Farrell, P. E. *A Framework for Automated PDE-constrained Optimisation*. 2013. arXiv: `1302.3894 [cs]`. Pre-published.

[114] Jiang, Z., Xu, T., and Wang, Y. "Enhancing Heat Production by Managing Heat and Water Flow in Confined Geothermal Aquifers". In: *Renew. Energy* 142 (2019), pp. 684–694.

[115] Liu, Y. et al. "Numerical Simulation and Design Optimization of Large-Scale Geothermal Production Based on a Multiwell Layout in Xianxian Geothermal Field". In: *Lithosphere* 2021 (Special 5 2022), p. 2929551.

[116] Lei, Z. et al. "Intermittent Thermal Extraction Optimization in Geothermal Heating Systems: A Case Study of Pei County, Jiangsu Province, China". In: *Energy Explor. Exploit.* (2025), p. 01445987241305155.

[117] Juliusson, E. and Horne, R. N. "Optimization of Injection Scheduling in Fractured Geothermal Reservoirs". In: *Geothermics* 48 (2013), pp. 80–92.

[118] Sun, J. et al. "Heat Extraction Strategies in Hongjiang Geothermal Field Insight from Numerical Simulation and Artificial Neural Network". In: *Earth Sci. Inf.* 18.2 (2025), pp. 422–436.

[119] Ansari, E., Hughes, R., and White, C. D. "Well Placement Optimization for Maximum Energy Recovery from Hot Saline Aquifers". In: *39th Workshop on Geothermal Reservoir Engineering, SGP-TR-202. Stanford: Stanford University.* 2014. URL: `https://pangea.stanford.edu/ERE/pdf/IGAstandard/SGW/2014/Ansari.pdf`.

[120] Garnett, R. *Bayesian Optimization*. Cambridge: Cambridge University Press, 2023.

[121] Wang, X. et al. "Recent Advances in Bayesian Optimization". In: *ACM Comput, Surv,* 55 (13s 2023), 287:1–287:36.

[122] Liu, Q. et al. "Hydraulic Fracturing Design in Geothermal Wells: A Utah FORGE Case Study". In: SPE Hydraulic Fracturing Technology Conference and Exhibition. OnePetro, 2025.

[123] Karimpouli, S. and Tahmasebi, P. "Physics Informed Machine Learning: Seismic Wave Equation". In: *Geosci. Front.* 11.6 (2020), pp. 1993–2001.

[124] Halilovic, S. et al. "Well Layout Optimization for Groundwater Heat Pump Systems Using the Adjoint Approach". In: *Energy Convers. Manage.* 268 (2022), p. 116033.

[125] Funke, S. W., Farrell, P. E., and Piggott, M. D. “Tidal Turbine Array Optimisation Using the Adjoint Approach”. In: *Renew. Energy* 63 (2014), pp. 658–673.

[126] Halilovic, S. et al. “Optimizing the Spatial Arrangement of Groundwater Heat Pumps and Their Well Locations”. In: *Renew. Energy* 217 (2023), p. 119148.